Orbit

4

J. Matthew Debnam, Jiawei Zhou, and Bita Esmaeli

Orbital lesions in both children and adults comprise a wide range of both benign and malignant tumors. The benign tumors include schwannomas and neurofibromas in patients with neurofibromatosis. Malignant tumors include lymphoma, rhabdomyosarcoma, and metastases. Other lesions such as idiopathic orbit inflammation, sarcoidosis, Graves' eye disease, and vascular lesions such as venous malformations may mimic orbital tumors both clinically and radiographically. Knowledge of the imaging features of these and other orbital tumors and diseases is important for patient care and to avoid permanent symptoms such as vision loss and other consequences.

The role of the radiologist is to assess the imaging appearance of an orbital lesion which may aid in narrowing the differential diagnosis, comment on benign versus malignant radiographic features, and describe the pattern and extent of disease spread including outside of the orbit and any involvement of the head and neck region. Specific imaging features to be mentioned in the radiology report include the size of the lesion, whether the lesion is well-circumscribed or infiltrative, whether there is mass effect upon the globe, the location in the intraconal or extraconal space, and the presence of bone remodeling or destruction of the orbital walls. In addition, the radiologist should assess specific ocular or periocular structures that are involved including the extraocular muscles, optic nerve, lacrimal gland, and orbital foramen.

The imaging modalities used for the evaluation of orbit include CT, MRI, PET/CT, and ultrasound. These modalities provide important information about staging, pre-surgical planning, and treatment response. CT aids in the delineation of tumor extent and bone remodeling or destruction. MRI can also be used to evaluate the features of the tumors including soft tissue characteristics, sinonasal and intracranial involvement, and perineural spread. PET/CT provides information for assessing a tumor's metabolic activity, detecting local and distant metastases, staging, determining a site for biopsy based on metabolic activity, and evaluating treatment response. Ultrasound is used to evaluate the parotid gland and neck for adenopathy and to guide fine-needle aspiration and core needle biopsy.

The purpose of this chapter is to describe the demographics and imaging appearance of common and uncommon malignancies and diseases of the orbit. This is accomplished with a review of the disease background, clinical presentation, and imaging features on various modalities and should provide the radiologist with a means to narrow their differential diagnosis. Tumors arising from the globe and cranial nerves, including the optic nerve, and those occurring secondarily from the bone and sinonasal cavities are discussed in other chapters.

Anatomy

Figure 4.1 shows schematic and imaging anatomy of the orbit.

- Retrobulbar orbit is located posterior to the globe.
- Divided into three compartments:

J. M. Debnam (✉)
Department of Neuroradiology, Division of Diagnostic Imaging, The University of Texas MD Anderson Cancer Center, Houston, TX, USA
e-mail: matthew.debnam@mdanderson.org

J. Zhou · B. Esmaeli
Department of Plastic Surgery, Division of Surgery, The University of Texas MD Anderson Cancer Center, Houston, TX, USA
e-mail: zzhou13@mdanderson.org; besmaeli@mdanderson.org

J. M. Debnam (ed.), *Imaging Atlas of Ophthalmic Tumors and Diseases*, https://doi.org/10.1007/978-3-031-17479-7_4

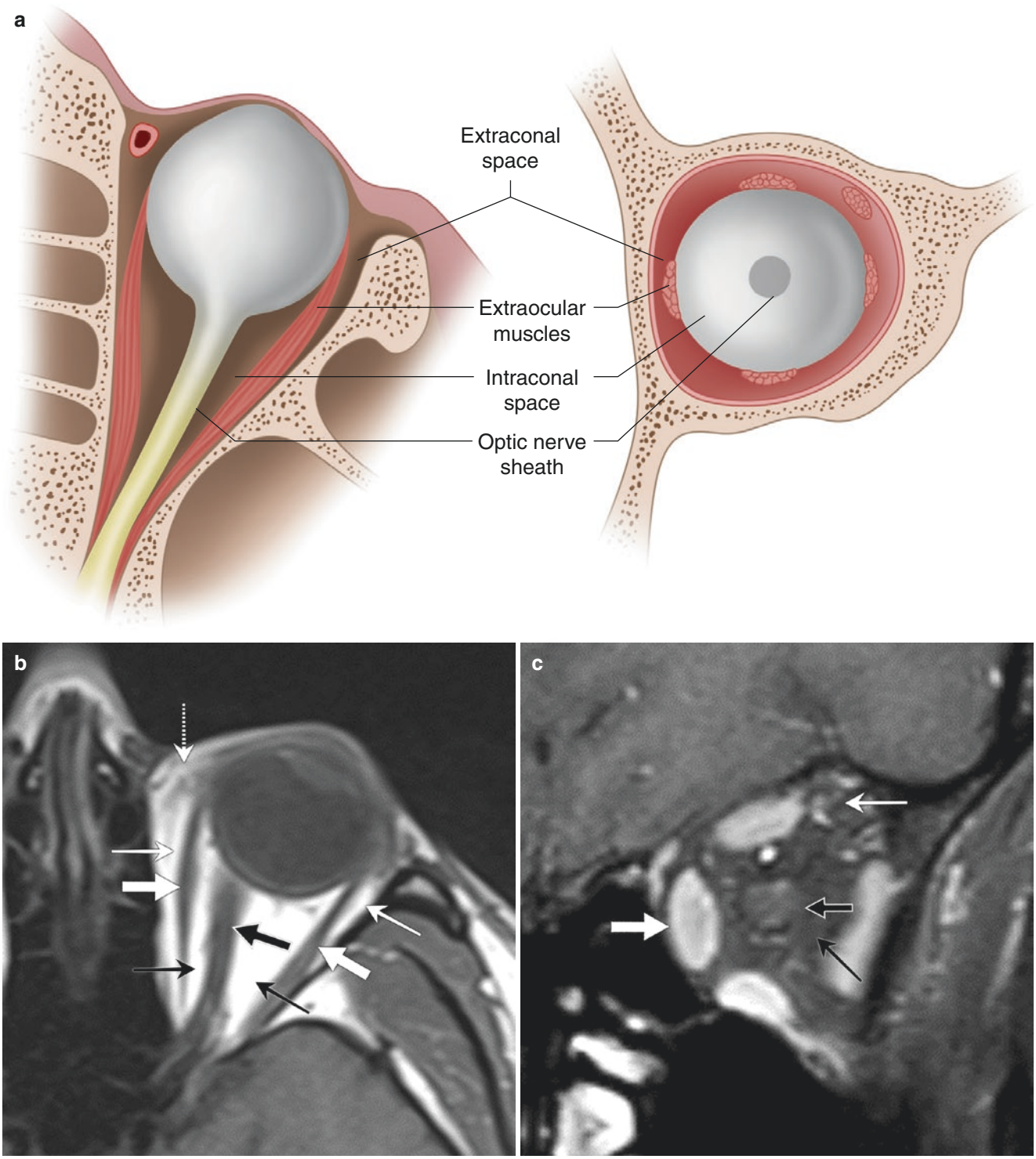

Fig. 4.1 Orbital anatomy. (**a**) Schematic drawing of the orbit demonstrating the intraconal and extraconal spaces. (**b**) Axial T1 non-contrast MRI without fat saturation shows the extraocular muscles (white arrows), optic nerve (black arrow), intraconal space (thin black arrows), extraconal space (thin white arrows), and the expected location or the orbital septum (dotted white arrow). (**c**) Coronal T1 post-contrast MRI with fat saturation shows the extraocular muscles (white arrow), optic nerve (black arrow), intraconal space (thin black arrow), and extraconal space (thin white arrow)

  - The muscle cone consists of the extraocular muscles excluding the inferior oblique muscle.
  - Intraconal space lies within the muscle cone.
  - Extraconal space lies outside the muscle cone.
- Extraocular muscles originate from the tendinous annulus of Zinn at the orbital apex and insert on the globe.
- Orbital septum: fibrous tissue originating from the periosteum of the orbital rim that blends superiorly with the tendon of the levator palpebrae superioris muscle and inserts inferiorly into the dense connective tissue of the eyelids (tarsal plates).

  Barrier between the preseptal and postseptal spaces.

Lymphoma

Figures 4.2, 4.3, and 4.4 show cases of orbital lymphoma.

Background

- **Most common malignancy of the orbit** [1, 2].
- Type of **non-Hodgkin lymphoma, mostly of the B-cell phenotype**.
- **Four subtypes**: extranodal marginal zone B-cell lymphoma (EMZL), diffuse large B cell lymphoma (DLBCL), follicular lymphoma (FL), and mantle cell lymphoma (MCL).
- **Most common subtype is EMZL**.
- **EMZL and FL have a better prognosis** than DLBCL and MCL [3].

Presentation

- Usually present in **adults without a gender bias**.
- **Most common presenting symptoms**: periorbital soft tissue swelling, mass, and proptosis.
- **Other symptoms**: epiphora (excessive tearing), pain, and diplopia [3].

Imaging

- Lymphoma usually **molds around or encases adjacent orbital structures** rather than causing mass effect.
- **Bone destruction is rare**; when present, these findings **suggest an aggressive histology**.
- **Occasionally, isolated extraocular muscle involvement or diffuse orbital infiltration may be seen** [4].

CT

- **Hyperdense mass** [4] with **homogeneous enhancement** [5].

MRI

- **T1 and T2 signal iso- to hypointensity** reflective of high cellularity.
- **Avid enhancement** following contrast administration [4].
- **Restricted diffusion** is often present on diffusion-weighed imaging (DWI) [6].

PET

- **High ^{18}F-FDG uptake** is noted on PET studies **except for low-grade MALT lymphoma,** which **can show low ^{18}F-FDG uptake** [7].
- Whole-body PET/CT is used for **staging** orbital lymphomas and **detection of systemic metastases** [8].

Key Points

- Comment on other sites of involvement.

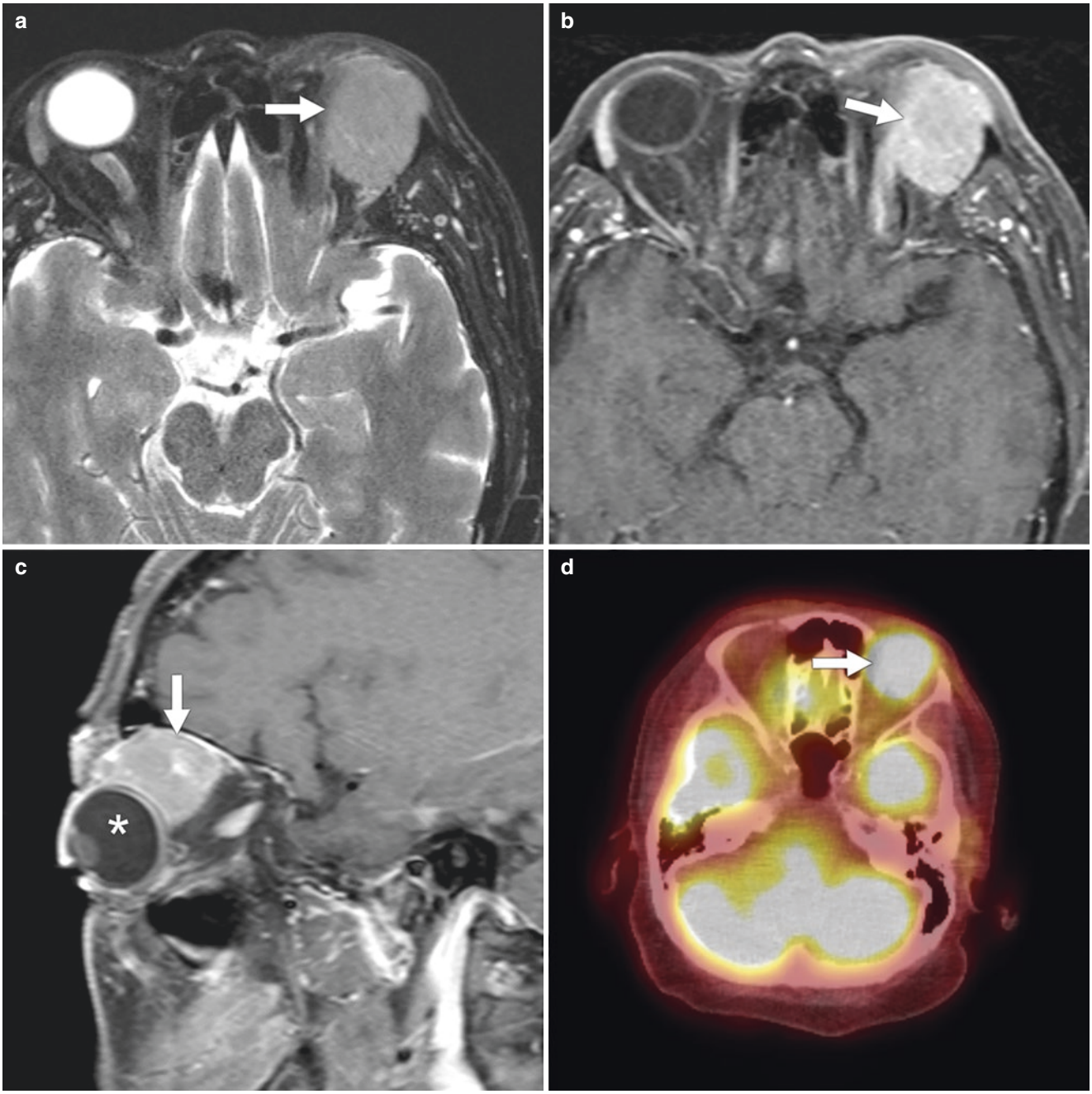

Fig. 4.2 A 68-year-old female with follicular lymphoma, left proptosis, and pain. (**a**) Axial T2 MRI with fat saturation shows a **homogeneously isointense appearance of follicular lymphoma in the superior left orbit** (arrow). (**b**, **c**) Axial and coronal T1 post-contrast MRI with fat saturation shows **homogeneous enhancement of the well-circumscribed, lobulated mass** (arrows). Note the **molding around the globe** (*) **that is displaced inferiorly**. (**d**) Axial ^{18}F-FDG PET/CT shows **FDG avidity of the left superior orbital lymphoma** (arrow)

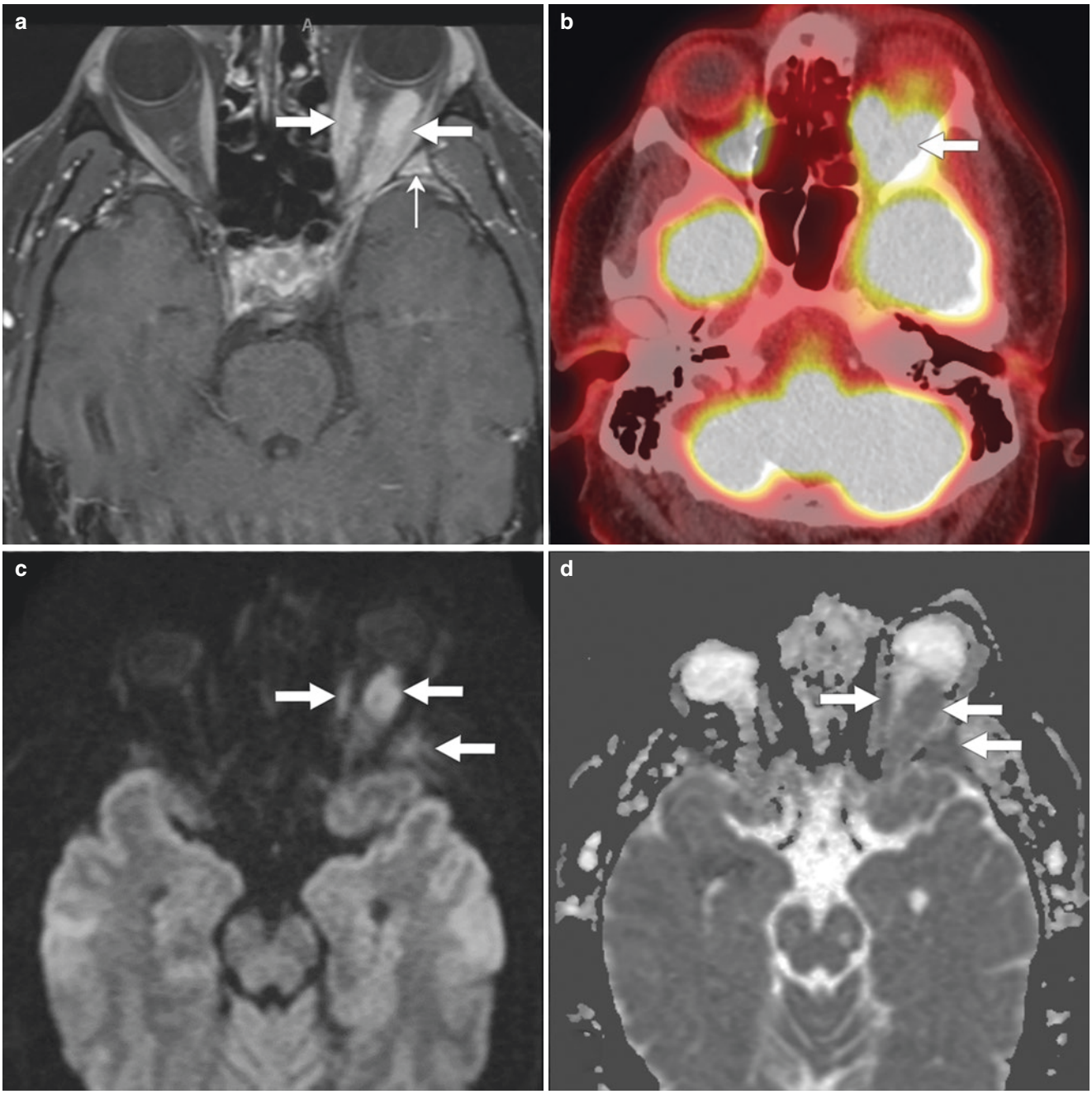

Fig. 4.3 A 51-year-old male with low-grade B cell lymphoma and left orbital proptosis. (**a**) Axial T1 post-contrast MRI with fat saturation shows a **homogeneously enhancing intraconal mass** in the left orbit (arrows). Note the **enhancement of the left sphenoid bone** (small arrow) (**b**) Axial ^{18}F-FDG PET/CT shows **FDG avidity of the left intraconal mass** (arrow). (**c**) DWI shows a **hyperintense signal in the left intraconal mass and sphenoid bone** (arrows). (**d**) Apparent diffusion coefficient map shows corresponding **hypointense signal in keeping with restricted diffusion of the lymphoma involving the left intraconal space and sphenoid bone** (arrows)

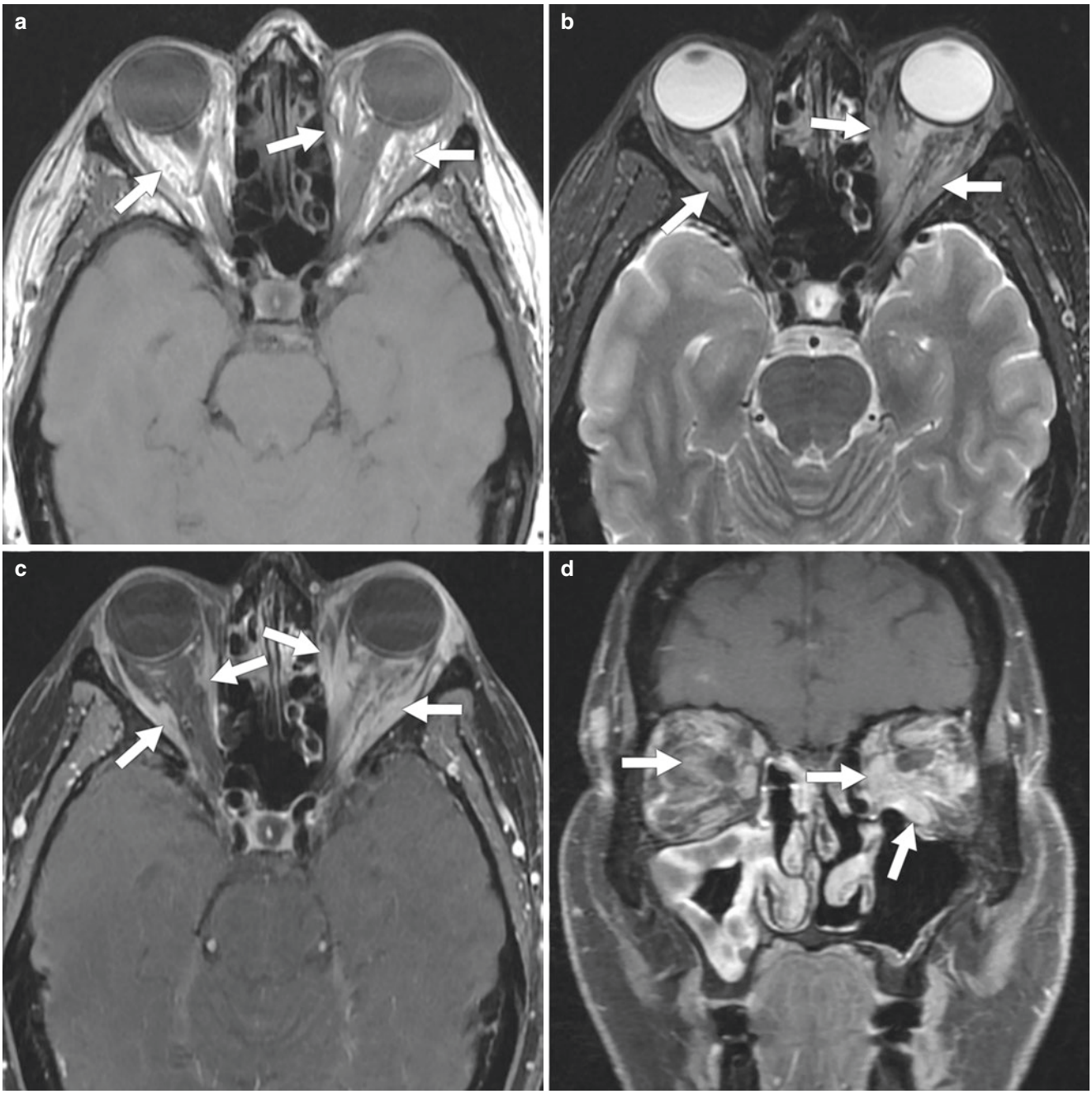

Fig. 4.4 A 56-year-old female with visual field defects and proptosis from orbital lymphoma. (**a**) Axial T1 non-contrast MRI without fat saturation shows **infiltrative soft tissue in the intraconal and extraconal spaces** in the left and right orbits (arrows). (**b**) Axial T2 MRI with fat saturation shows an **isointense infiltrative appearance of lymphoma in the orbits** (arrows). (**c**, **d**) Axial and coronal T1 post-contrast MRI with fat saturation show **enhancing infiltrative lymphoma in the intraconal and extraconal spaces with enlargement of the EOMs** (arrows)

Leukemia

Figures 4.5 and 4.6 show cases of orbital leukemia.

Background

- Leukemia is a **disorder of hematopoietic stem cells in the bone marrow** [9].
- **Lymphoid leukemia** affects white blood cells (too many lymphocytes).
- **Myeloid leukemia** affects cells that give rise to white blood cells (other than lymphocytes), red blood cells, and platelets.
- **Extramedullary deposits** of lymphocytic and myelogenous precursor cells can be found in any organ [10].
- **Ocular manifestations** occur **more commonly with myeloid leukemia** as opposed to lymphoid leukemia [11, 12] and **most commonly involve the retina** [9].
- **Granulocytic sarcoma**, also known as myeloid sarcoma and previously as chloroma, is a **solid tumor** of primitive granulocytes, vascular stroma, and connective tissue occurring in patients with **myelogenous leukemia** [13].
- **Orbital granulocytic sarcoma** is rare in adults and **more commonly present in pediatric patients** [14].

Presentation

- **The globes and orbits are the third most common site after the meninges and testes** [15].
- Ocular involvement can precede the diagnosis or can occur during the disease [16].
- **Central nervous system (CNS) involvement** may include **cranial nerve infiltration and palsies as well as papilledema** [9].

Imaging

- **Homogenous mass that molds to the orbit** [10].
- Usually **encases rather than invading structures**.
- **May also appear as infiltrative disease.**
- Bone erosion, demineralization, and periosteal reaction occur less commonly.
- **Granulocytic sarcoma** usually presents as a **soft-tissue mass in the lateral orbital wall that may have infiltrative borders** [13].

CT

- **Isointense or slightly hyperintense** and **demonstrates mild homogeneous enhancement** [10].
- There may be **invasion of the orbital fat** and extension to involve the eyelid.
- Calcification is not present.
- **Granulocytic sarcomas** are **homogeneously isodense to slightly hyperdense with homogeneous enhancement** [13].

MRI

- **T1 slightly hyperintense and T2 isointense** [17].
- **Granulocytic sarcoma** is **T1 iso- to hypointense, T2 heterogeneously iso- to hyperintense, and homogeneously enhancing** [13].

PET

- **Orbital leukemia is ^{18}F-FDG- avid**. PET/CT is sensitive for the detection of granulocytic sarcoma and additional sites of disease [18].

Key Points

- Comment on other sites of involvement.

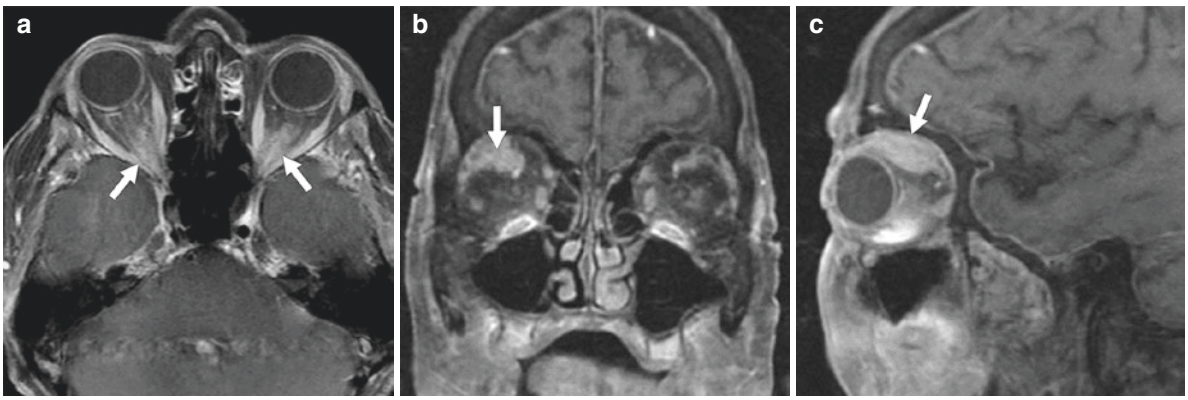

Fig. 4.5 (**a**) An 82-year-old female with acute myeloid leukemia who presented with diplopia, pain, and restriction of movement of the globes. (**a**) Axial T1 post-contrast MRI with fat saturation shows **infiltrative disease in the orbital apex bilaterally** (arrows). (**b**, **c**) A 78-year-old female with relapsed acute myeloid leukemia. (**b**, **c**) Axial and coronal T1 post-contrast MRI with fat saturation show **solid, homogeneously enhancing granulocytic sarcoma in the superior right orbit and superior rectus-levator muscle complex** (arrows)

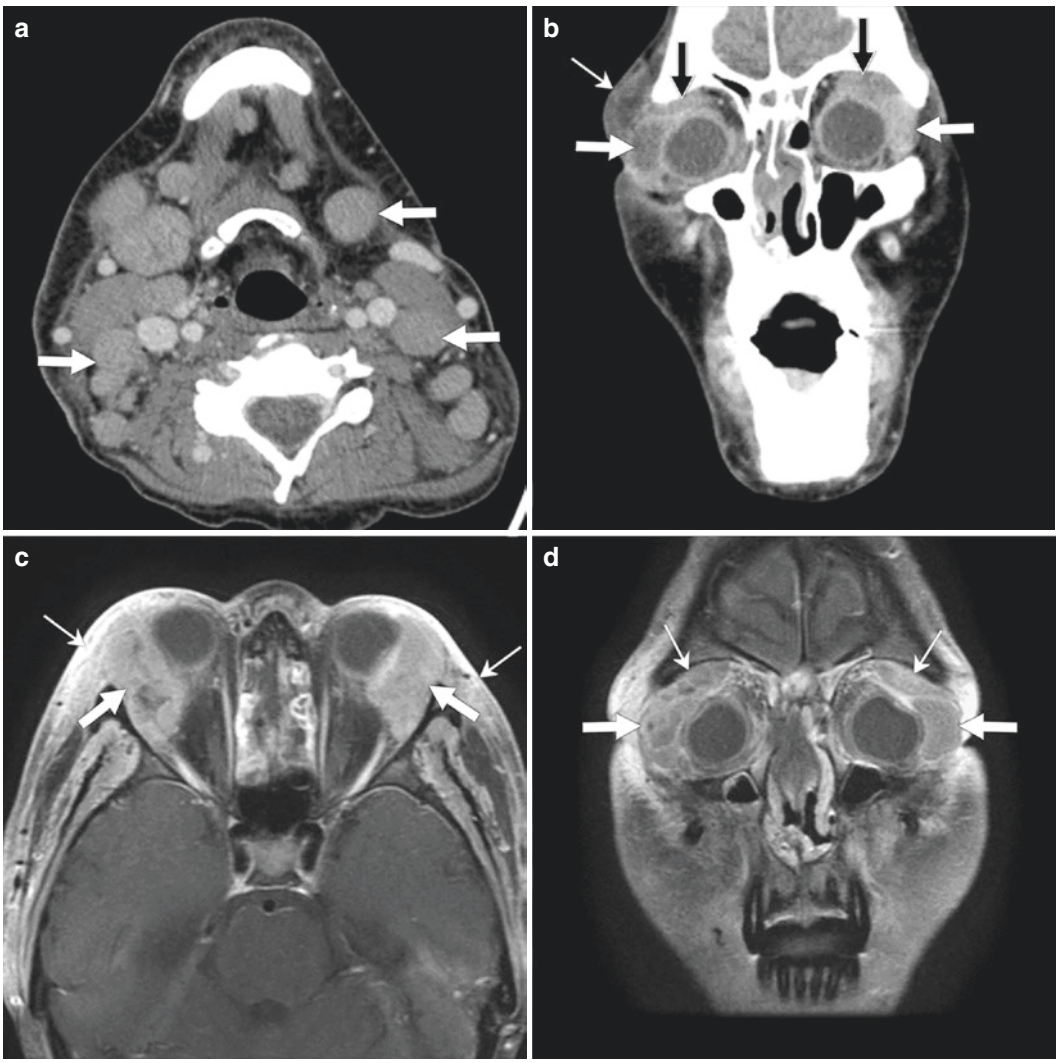

Fig. 4.6 A 25-year-old male with T-cell acute lymphoid leukemia who presented with right periorbital swelling. (**a**) Axial CT with contrast, soft tissue window shows **extensive bilateral neck adenopathy** (arrows). (**b**) Coronal CT with contrast, soft tissue window shows **enlargement of bilateral lacrimal glands** (white arrows) **with disease in the superior orbits** (black arrows) and the presence of **right periorbital soft tissue infiltration** (thin white arrow). (**c**) Axial T1 post-contrast MRI with fat saturation shows **enlargement of bilateral lacrimal glands** (arrows) and **bilateral periorbital soft tissue infiltration** (white arrows). (**d**) Coronal T1 post-contrast MRI with fat saturation shows **enlargement of bilateral lacrimal glands** (arrows) **and disease in the superior orbits** (thin arrows)

Rhabdomyosarcoma

Figure 4.7 shows cases of orbital rhabdomyosarcoma.

Background

- RMS is **a tumor of striated muscle or mesenchymal cell precursors** [19, 20].
- **Most common childhood malignancy of the orbit,** accounting for 10% of all cases of RMS [21, 22].
- Two most commonly encountered subtypes: **embryonal and alveolar**.
- Orbital RMS occurs **less frequently in the adult population** [23].
- **RMS may arise from adjacent structures, including the sinonasal cavity, and spread to the orbit** [24].

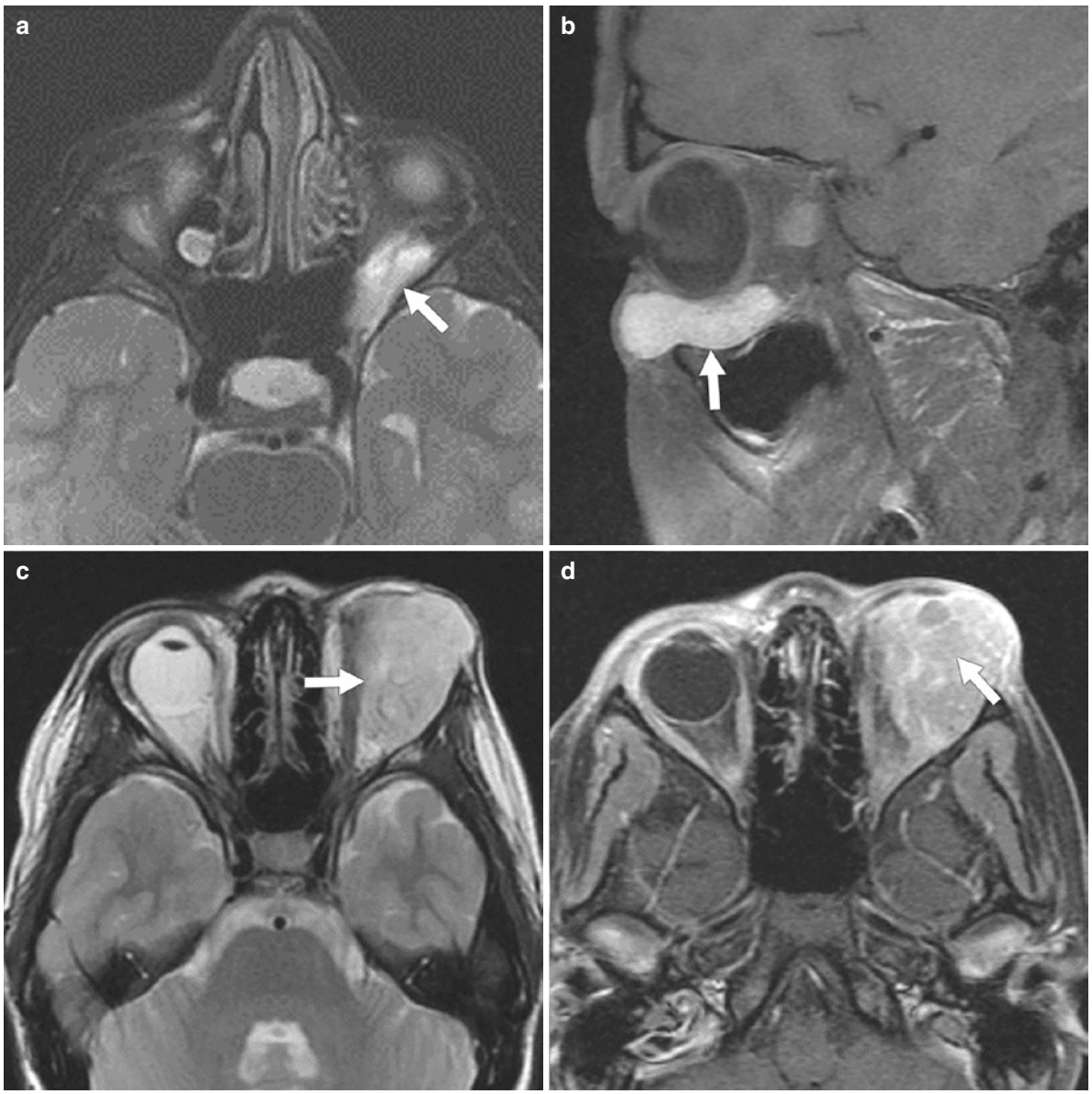

Fig. 4.7 (**a**, **b**) A 6-year-old male with left orbital embryonal rhabdomyosarcoma. (**a**) Axial T2 MRI with fat saturation shows a **homogeneously hyperintense mass in the inferior left orbit** (arrow). (**b**) Sagittal T1 post-contrast MRI with fat saturation shows **homogeneous enhancement of the well-circumscribed left inferior orbital mass** (arrow). (**c**, **d**) A 13-year-old female with left orbital swelling due to an embryonal rhabdomyosarcoma. (**c**) Axial T2 MRI with fat saturation shows a **heterogeneously isointense mass in the superior left orbit** (arrow). (**d**) Axial T1 post-contrast MRI with fat saturation shows **heterogeneous enhancement** of the left superior orbital rhabdomyosarcoma. Note **small rings of enhancement** within the mass (arrow)

Presentation

- In the **pediatric population,** RMS presents with **visible signs such as an orbital mass, periorbital soft tissue swelling, proptosis, or blurry vision**.
- In the **adult population, secondary signs such as sinus congestion and infection are more common than an orbital or sinonasal mass** [25].

Imaging

- **Usually appears as a soft-tissue mass**.
- **Imaging features similar to other soft tissue sarcomas** [23].
- **Calcification, hemorrhage, and necrosis are uncommon** [24].
- **Eyelid thickening** and **bone thinning or destruction** in up to 40% of cases.
- RMS may **extend into adjacent paranasal sinuses or intracranially.**
- **Predictors of poor outcome**: tumor invasiveness, regional lymph node involvement, metastasis, and older age at diagnosis [25].

CT

- Orbital RMS appears as a **well-circumscribed mass that is isodense to muscle with moderate to marked enhancement** [26].

MRI

- **T1 isointense and T2 hyperintense to muscle.**
- **Moderate to marked and homogeneous to heterogeneous enhancement** [26].
- **Thin rings of enhancement have been described** [24].

Key Points

- **Try to determine the primary location of the tumor**, e.g., in the orbit or sinuses.
- Assess for **regional lymph node involvement**.

Schwannoma

Figures 4.8 and 4.9 show cases of orbital schwannomas.

Background

- Benign nerve sheath tumors comprised of spindle cells arranged as **compact** (**Antoni type A)** or **loose (Antoni type B)** tissues [27].
- The **more commonly involved nerves** about the orbit are the **trigeminal (CN V) and facial (CN VII) nerves**.
- **Soft tissue sarcomas** that originate from the peripheral nerve sheath are termed **malignant peripheral nerve sheath tumors (MPNSTs**) [28].

Presentation

- **Denervation-induced muscle atrophy or a sensory deficit** can aid in identifying the cranial nerve of origin or occurs if an adjacent cranial nerve is affected from long-standing mass effect [29].
- **Clinical symptoms that suggest transformation to an MPNST**: non-specific symptoms including new pain, increased growth, and new neurologic deficits [30].

Imaging

- **Slow growth** of a schwannoma is characterized by **smooth expansion of an affected neural foramen, bone remodeling, and/or mass effect on adjacent soft tissues** [29, 31].

CT

- Cranial nerve schwannomas demonstrate **variable enhancement** [31, 32].

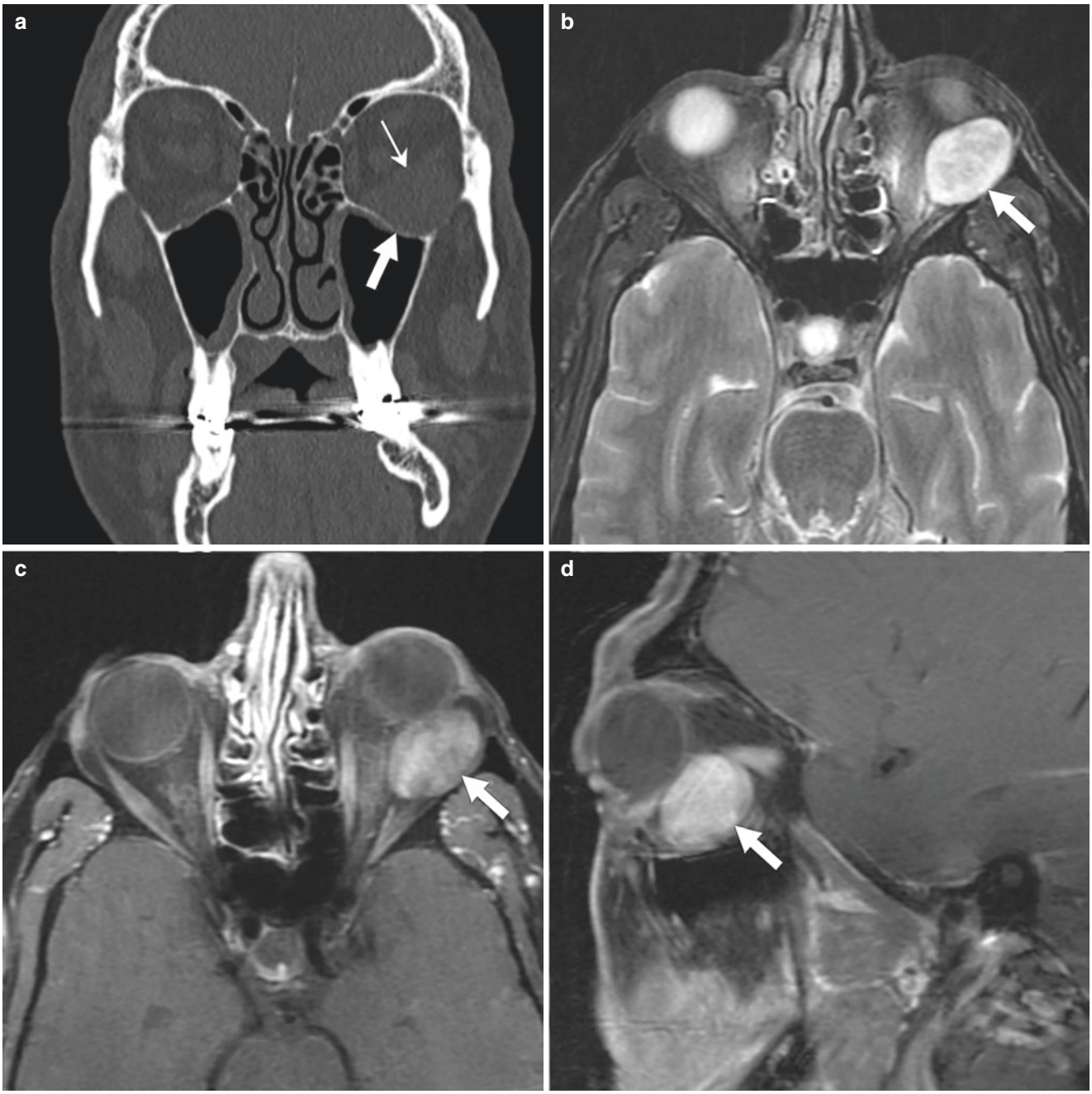

Fig. 4.8 A 65-year-old male with left exophthalmos due to an orbital schwannoma. (**a**) Axial CT with contrast, bone window shows **subtle remodeling of the left orbital floor** (arrow) **adjacent to a mass** (thin arrow). (**b**) Axial T2 MRI with fat saturation shows a **heterogeneously hyperintense, well-circumscribed schwannoma** in the inferolateral left orbit (arrow). (**c**, **d**) Axial and sagittal T1 post-contrast MRI with fat saturation show **heterogeneous enhancement** of the schwannoma (arrows)

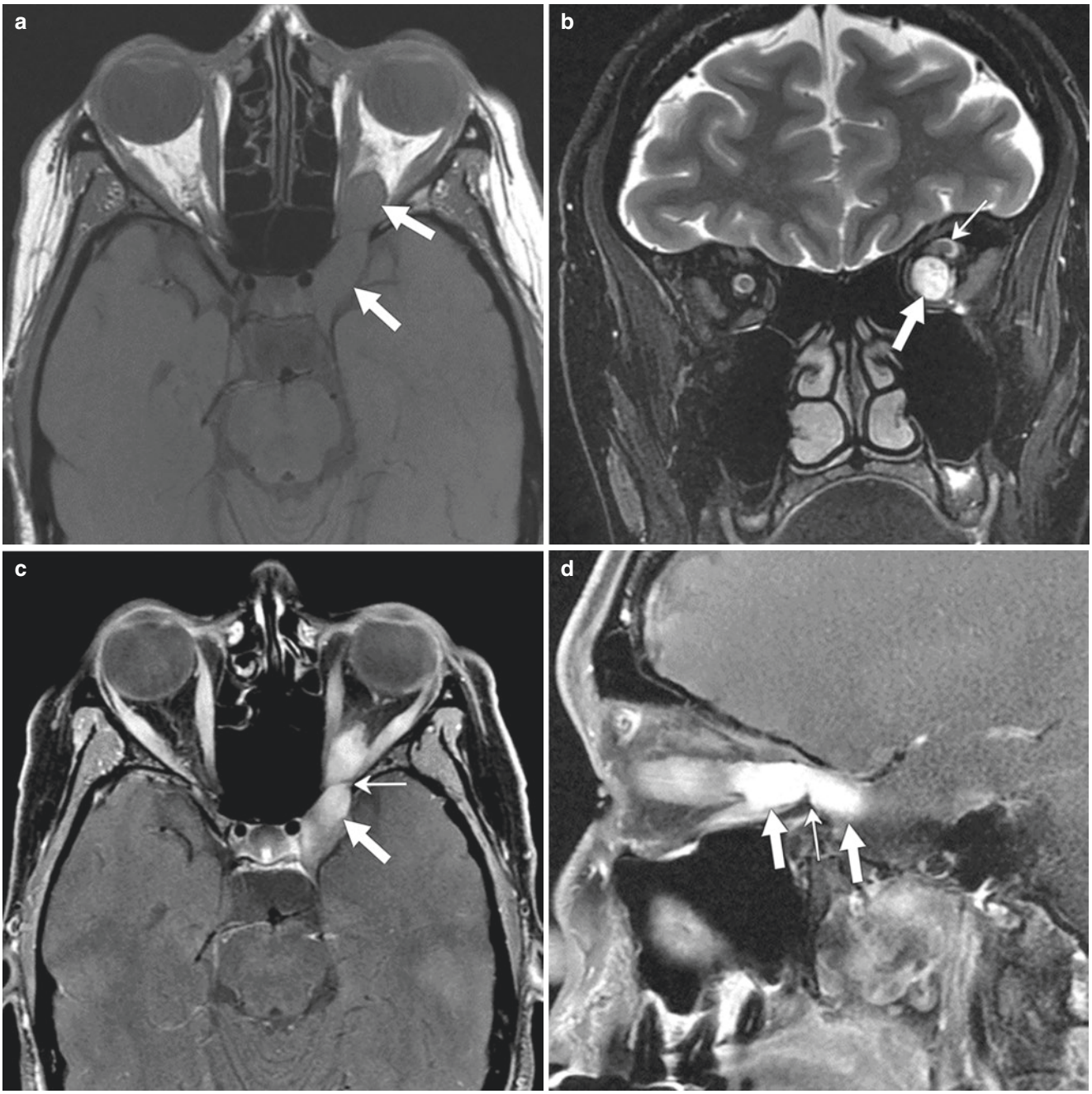

Fig. 4.9 A 34-year-old female with an incidentally discovered left orbital schwannoma. (**a**) Axial T1 non-contrast MRI without fat saturation shows a **well-circumscribed homogeneous appearance of the left orbital schwannoma** (arrows). (**b**) Coronal T2 MRI with fat saturation shows a **hyperintense appearance of the schwannoma** (arrow) with **superotemporal displacement of the optic nerve** (thin arrow). (**c**, **d**) Axial and sagittal T1 post-contrast MRI with fat saturation show **homogeneous enhancement of the schwannoma** (arrow) that is **narrowed as it passes through the superior orbital fissure** (thin arrow)

MRI

- **Appearance depends on the components of Antoni type A and B tissues** [27].
- **T1 hypo- to isointense with avid enhancement**.
- **T2 heterogeneously hyperintense** due to **compactly arranged cells (Antoni type A pattern-hypointense)** intermixed with areas of **loosely arranged cells (Antoni type B pattern-hyperintense)** with variable water content and cellularity [27, 33] thus **can be hypo- to isointense** [34].
- **Larger lesions may demonstrate heterogeneous enhancement, internal cysts, and hypointense foci of hemosiderin** related to internal hemorrhage [29].
- **MRI findings of MPNSTs**: larger size, heterogeneous signal and enhancement, internal necrosis without enhancement, irregular margins, and local invasion [34].
- **Restricted diffusion associated with MPNSTs** has been described [34]; however, further work on this topic is needed [28].

PET

- In addition to **intense ^{18}F-FDG avidity**, both schwannomas and MPNSTs may have a large size and demonstrate a heterogeneous appearance [34].

Key Points

- **Attempt to determine which nerve is involved**.
- Describe **orbital foraminal involvement** e.g., superior orbital fissure, foramen rotundum.

Solitary Fibrous Tumor

Figures 4.10, 4.11, and 4.12 show cases of orbital solitary fibrous tumors.

Background

- A solitary fibrous tumor (SFT) , formerly named hemangiopericytoma [35], is a **spindle-cell neoplasm** that originates from mesenchymal tissue and most frequently occurs in the pleura [36].
- Increasing incidence has been noted in extra-pleural sites, including the head and neck, chest, abdomen, pelvis, and meninges [37, 38].
- SFTs may occur in the **postseptal orbit, lacrimal gland and sac, and lower eyelid** [36, 37].

Presentation

- **Wide age range**: from 9 to 76 years; no gender predilection [39, 40].
- **Symptoms**: slowly progressive exophthalmos or palpable mass [41].

Imaging

- SFTs present as **well-defined, ovoid masses.**
- **More common in the superolateral or superomedial orbit followed by the inferomedial orbit** [42].

CT

- SFTs are **isodense to slightly hyperdense** on non-contrast CT [42, 43].
- **Rapid enhancement** following contrast administration [42].

MRI

- Generally **T1 homogeneously isointense** [43].
- **T1 hypointense components** are related to **cystic or myxoid degeneration** [44].
- **T2 isointense to hypointense** related to **fibrous tissue** with a large collagen content.
- **Areas of fresh fibrosis, internal hemorrhage, and cystic degeneration may be T2 hyperintense** [42].
- **Signal flow voids** from vessels may be noted [43].
- **Areas of T2 hyperintensity with strong enhancement** have been described as suggestive of an SFT [45].
- **Rapid enhancement with a washout pattern of contrast** may aid in diagnosis [42].
- **Slight restricted diffusion** has been reported [41].

Key Points

- T2 hypointense with rapid uptake of contrast.
- **Signal flow voids** from vessels may be present.

Fig. 4.10 A 39-year-old male with left proptosis due to a solitary fibrous tumor. (**a**) Axial CT with contrast, bone window shows a **mass in the left posterior orbit with widening of the superior orbital fissure** (arrow). (**b**) Axial T2 MRI with fat saturation shows a **heterogeneous, predominately hypointense mass in the left orbital apex** (arrow). (**c**, **d**) Axial and coronal T1 post-contrast MRI with fat saturation shows **small hypointense vascular flow voids** (arrows) **coursing through the homogeneously enhancing mass**

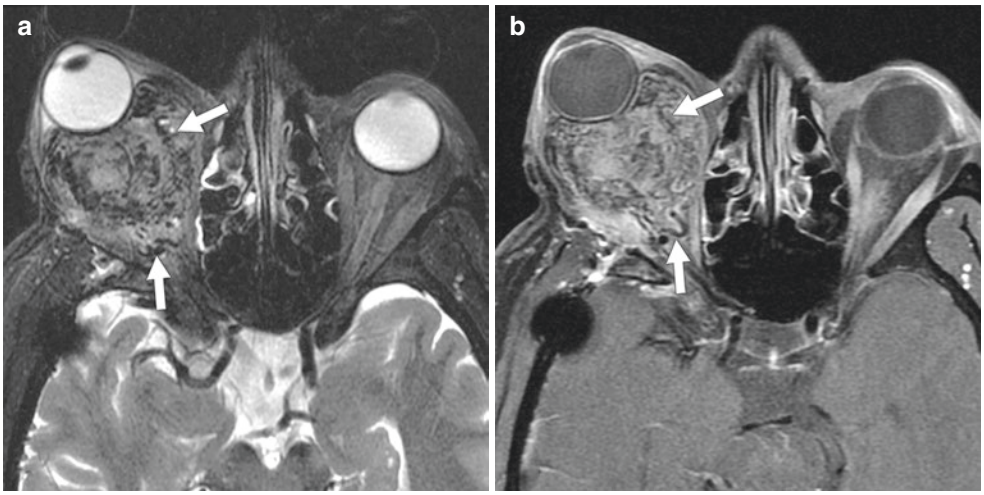

Fig. 4.11 A 65-year-old male with right proptosis and orbital pain related to a solitary fibrous tumor. (**a**) Axial T2 MRI with fat saturation shows a **right orbital heterogeneous intraconal mass with hypo- to isointense signal and multiple vascular flow voids** (arrows) and **proptosis** of the globe. (**b**) Axial T1 post-contrast MRI with fat saturation shows **heterogeneous enhancement of the tumor with multiple vascular flow voids** (arrows)

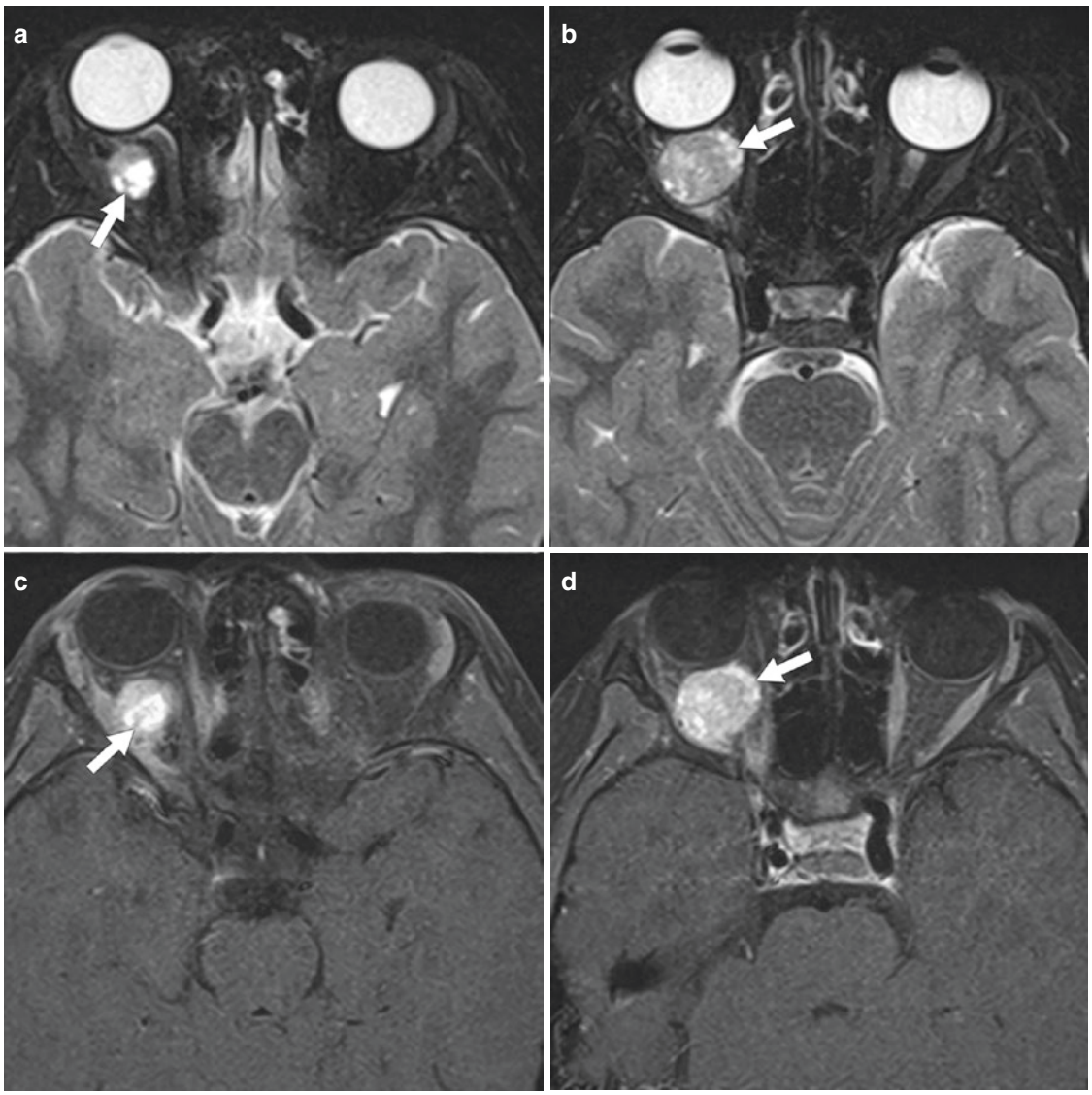

Fig. 4.12 An 8-year-old male with right lower eyelid swelling after trauma and an incidental solitary fibrous tumor. (**a**, **b**) Axial T2 MRI with fat saturation shows a **well-circumscribed intraconal mass with iso- to hyperintense signal** (arrows). (**c**, **d**) Corresponding Axial T1 post-contrast MRI with fat saturation shows **more solid enhancement in the regions of the tumor that are hyperintense on the T2-weighted series** (arrows)

Liposarcoma

Figure 4.13 shows a case of an orbital liposarcoma.

Background

- Tumor with **differentiation of malignant lipoblasts** [46, 47].
- **Five histologic subtypes:** well-differentiated, dedifferentiated, myxoid, pleomorphic, and mixed [46–48].
- The **majority occur** in the **deep soft tissues of the retroperitoneum and extremities** with a small percentage occurring in the head and neck [49].

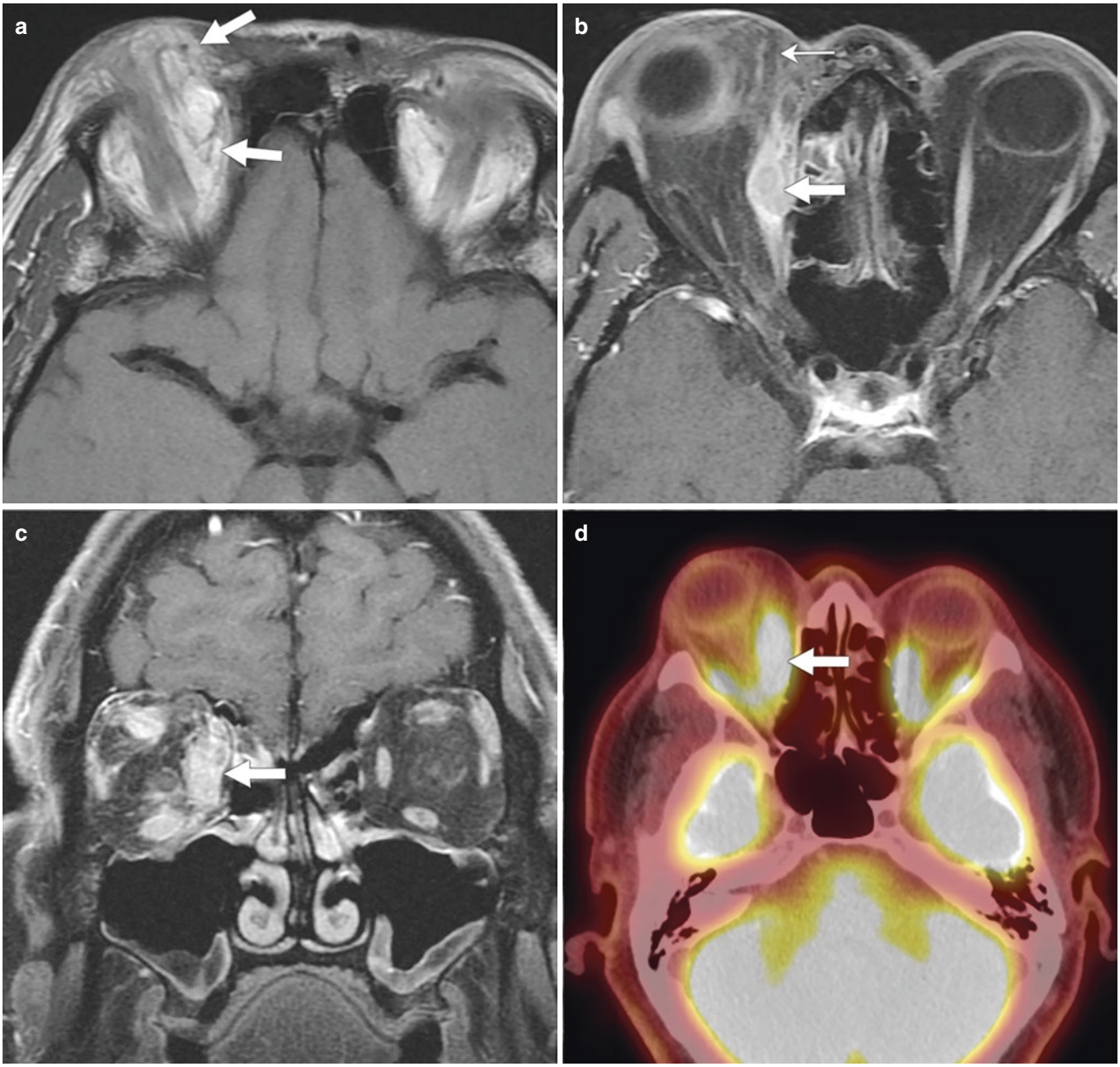

Fig. 4.13 A 44-year-old male with a right orbital liposarcoma. (**a**) Axial T1 non-contrast MRI without fat saturation shows a **hyperintense mass in the superonasal right orbit** (arrows). (**b**, **c**) Axial and coronal T1 post-contrast MRI with fat saturation shows **enhancement of the solid component of the liposarcoma** (arrows) and **suppression of fat signal in the fatty component** (thin arrow). (**d**) Axial ^{18}F-FDG PET/CT shows **FDG avidity of the solid component** of the liposarcoma (arrow)

Presentation

- More common in **males in the fourth through sixth decades**.
- **Painless soft tissue mass** [46, 47].

Imaging

- Liposarcomas **contain fat similar to lipomas, with variable amounts of associated soft tissue**.

CT

- **Hypodense component similar to a lipoma with variable soft tissue densities**.
- **Intratumoral calcification and internal bleeding** lead to a **hyperdense appearance** [46, 50].

MRI

- **Well-differentiated liposarcoma** appears **similar to a benign lipoma with T1 hyperintense and T2 iso- to hypointense signal and minimal to no contrast enhancement**.
- **Less well-differentiated subtypes** (pleomorphic, myxoid) show **T1 hypointense tissue with septa and scattered islands of fatty T1 hyperintense tissue.**
- In these cases, the **solid components of the mass are T2 iso- to hyperintense with an iso- to hypointense appearance of the fatty tissue**.
- **Stromal enhancement is present in less well-differentiated subtypes** [51].

PET

- **Well-differentiated liposarcomas show low ^{18}F-FDG avidity** reflective of a low malignant potential while **less well-differentiated subtypes show marked ^{18}F-FDG uptake** [49].

Key Points

- Search for **soft tissue associated with the fat component**.

Orbital Metastases

Figures 4.14, 4.15, 4.16, 4.17, 4.18, and 4.19 show cases of orbital metastases.

Background

- Tumors that metastasize to the obit represent between **2.5 and 10% of all orbital mass lesions** [52].
- Approximately 35% of patients with an orbital metastasis do not have a history of a primary tumor at the time of diagnosis [53].
- The **most common primary tumor sites** are the **breast, lung, prostate, and malignant melanoma** arising from the skin [54, 55].
- **In children, orbital metastases** arise from metastatic **neuroblastoma, Wilms' tumor, and Ewing's sarcoma** [56].

Presentation

- **Symptoms**: proptosis, diplopia, decreased vision, eyelid swelling, conjunctival swelling (chemosis), and redness [57].

Imaging

- Metastases can be **intraconal or extraconal** [58, 59] **or involve the extraocular muscles (EOMs)** with enlargement of the involved muscle [60].
- **Variety of appearances from nodular to diffusely infiltrative**.
- **Single or multiple; usually unilateral but can be bilateral** [57].
- Extension into the **intracranial compartment** or **paranasal sinuses** may also occur.

CT

- **Isodense on non-contrast CT and demonstrates enhancement**.

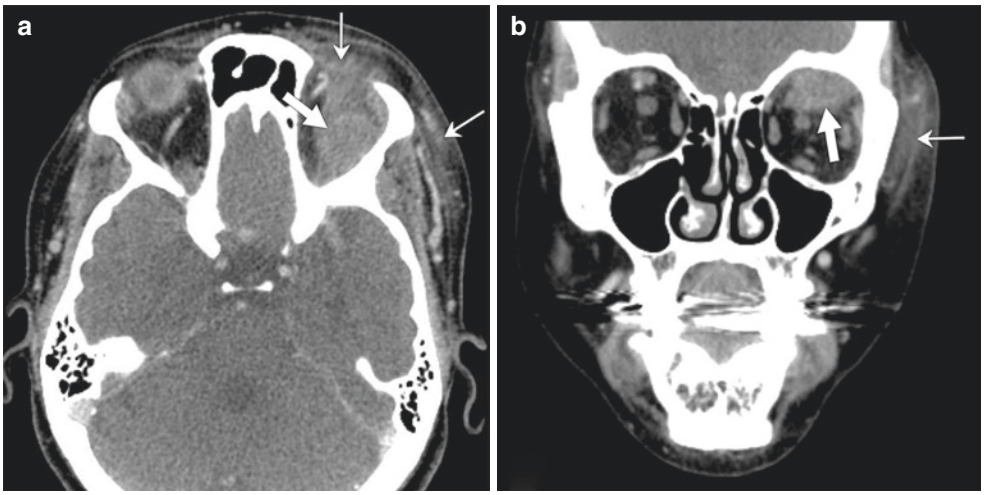

Fig. 4.14 A 49-year-old female with carcinoma of the anal canal who presented with left periorbital erythema and ophthalmoplegia (weakness of the EOMs). (**a**, **b**) Axial and coronal CT with contrast, soft tissue window shows a **solid metastasis in the posterior superior left orbit** (arrows) with soft tissue standing in the anterior left orbital and periorbital soft tissues from **unrelated cellulitis** (thin arrow)

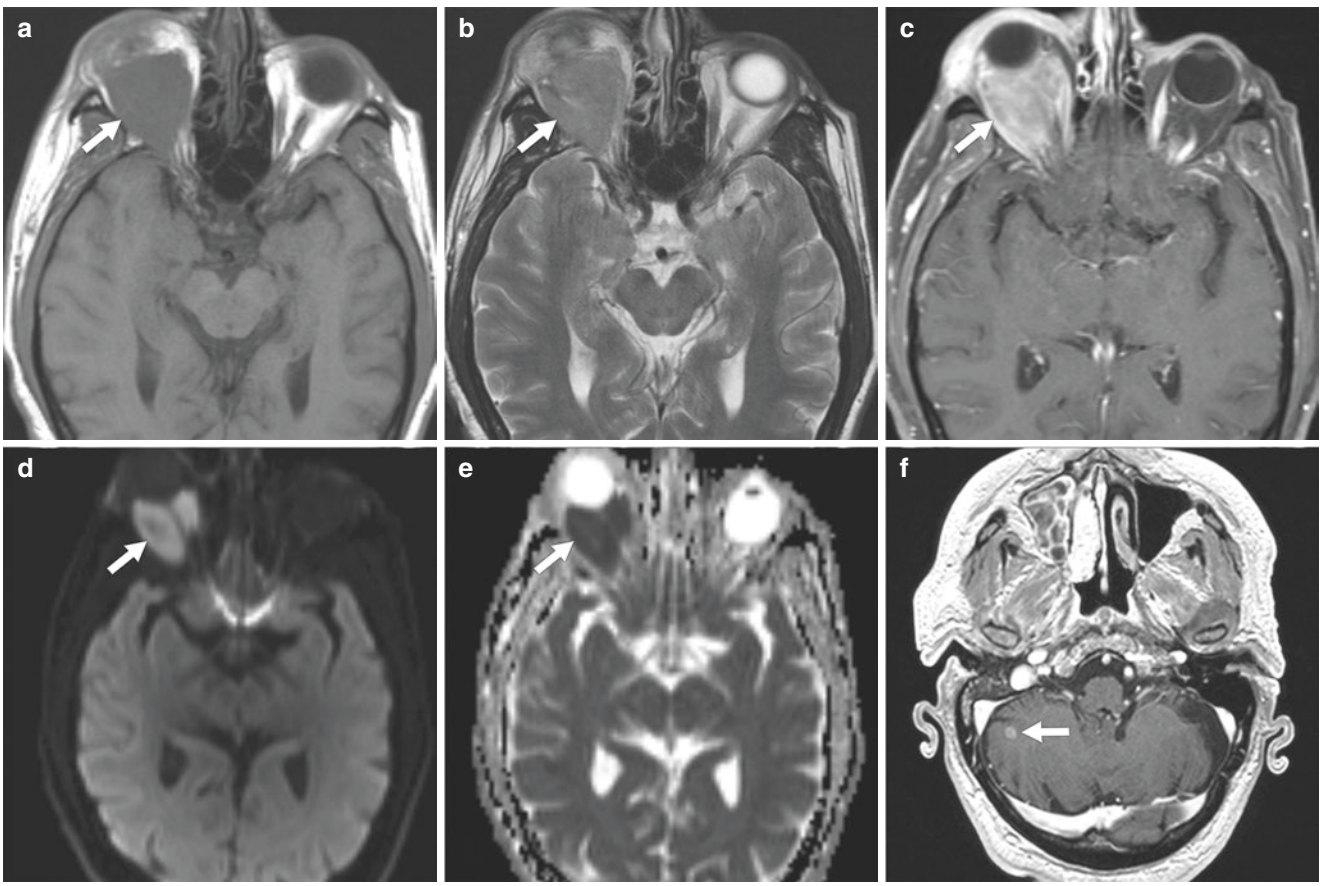

Fig. 4.15 A 61-year-old male with melanoma who presented with right proptosis and diplopia. (**a**) Axial T1 non-contrast MRI without fat saturation shows an **isointense appearance of the right orbital mass** (arrow). (**b**) Axial T2 MRI with fat saturation shows an **isointense right orbital metastasis** (arrow). (**c**) Axial T1 post-contrast MRI with fat saturation demonstrates **heterogeneous enhancement of the orbital melanoma** (arrow). (**d**) DWI shows **hyperintense signal** in the right orbital melanoma (arrow). (**e**) Apparent diffusion coefficient map shows corresponding **hypointense signal in the mass consistent with restricted diffusion** (arrow). (**f**) Axial T1 post-contrast MRI without fat saturation shows a **small right cerebellar metastasis** (arrow)

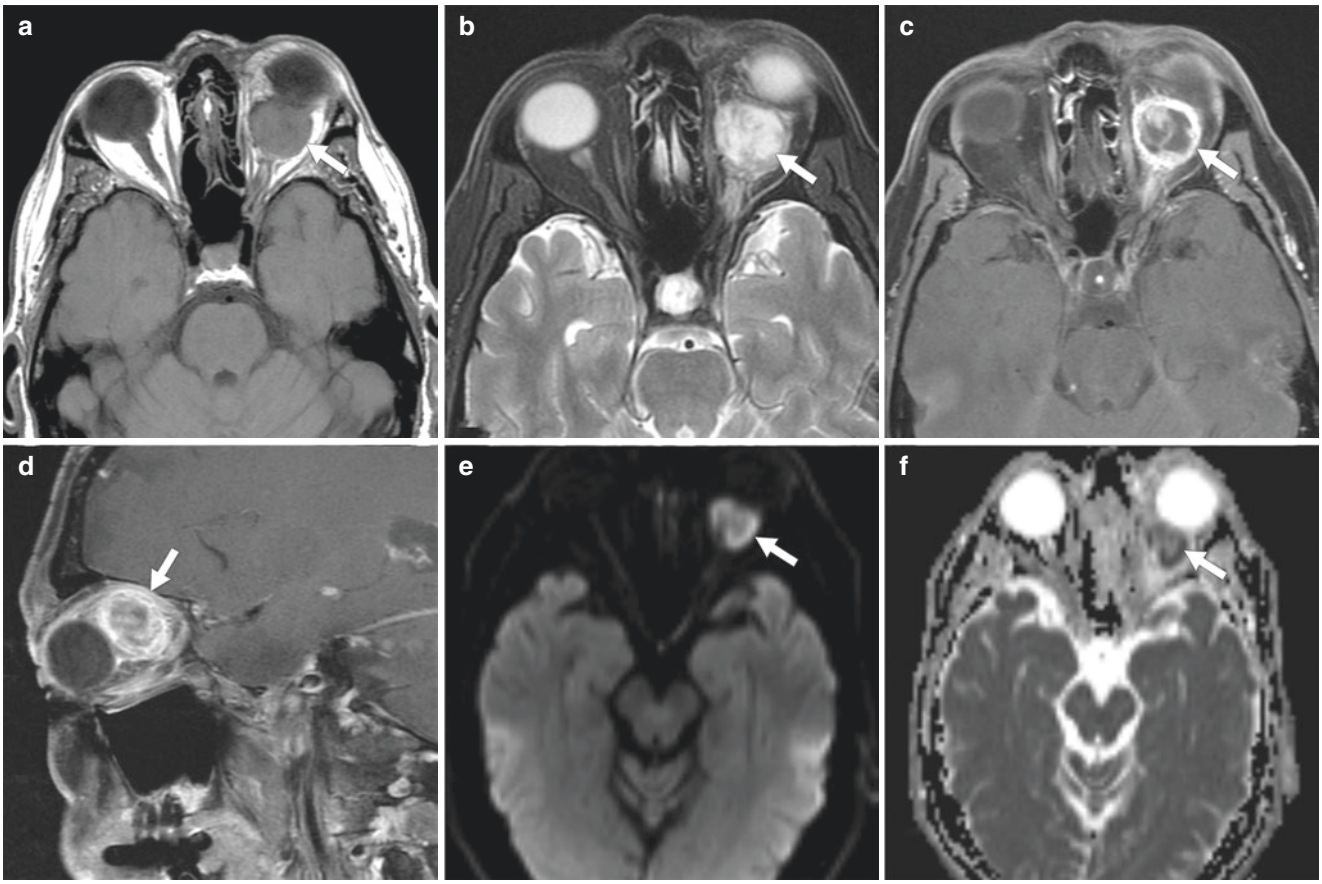

Fig. 4.16 A 74-year-old male with melanoma and left proptosis. (**a**) Axial T1 non-contrast MRI without fat saturation shows an **isointense intraconal metastasis in the left orbit** (arrow). (**b**) Axial T2 MRI with fat saturation shows **predominately hyperintense signal in the metastasis** (arrow). (**c**, **d**) Axial and coronal T1 post-contrast MRI with fat saturation show **peripheral enhancement** (arrows). (**e**) DWI shows **hyperintense signal in the lesion** (arrow). (**f**) Apparent diffusion coefficient map shows corresponding **hypointense signal in the metastasis in keeping with restricted diffusion** (arrow)

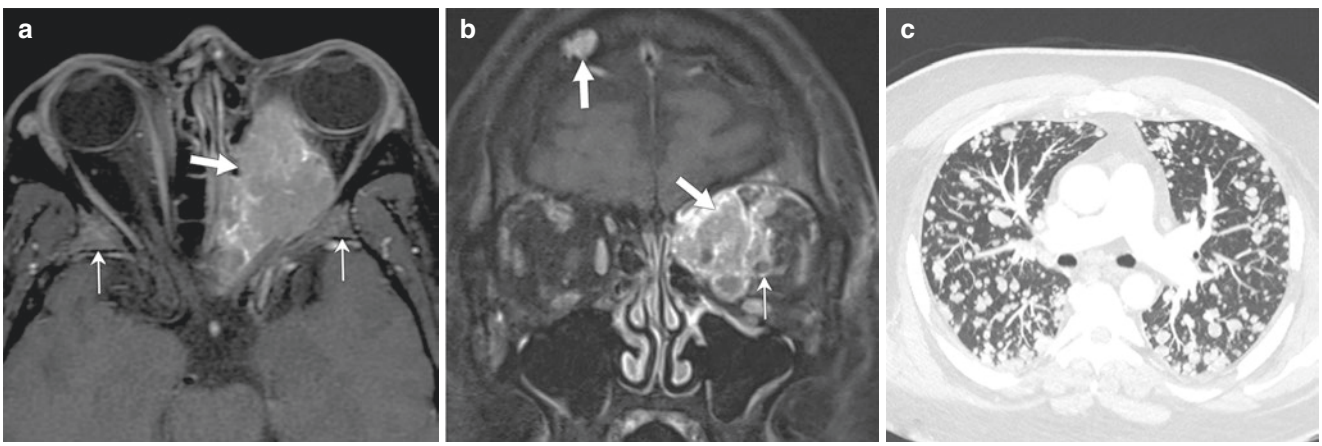

Fig. 4.17 A 42-year-old male with recurrent glomus tumor, left orbital pain, and vision loss. (**a**) Axial T1 post-contrast MRI with fat saturation demonstrates an **intraconal and extraconal left orbital mass with extension to the orbital apex and into the ethmoid air cells** (arrow). Note **metastases involving the sphenoid bones bilaterally** (thin arrows). (**b**) Coronal T1 post-contrast MRI with fat saturation shows the **intraconal and extraconal left orbital mass and a right frontal calvarial metastasis** (arrows). Note **inferolateral displacement of the optic nerve** (thin arrow). (**c**) Axial CT without contrast, lung window shows **numerous pulmonary metastases**

Fig. 4.18 A 63-year-old male with renal cell carcinoma who presented with right proptosis due to an orbital metastasis. (**a**) Axial T1 non-contrast MRI without fat saturation shows an **isointense metastasis in the right lateral rectus muscle** (arrow). (**b**) Axial T2 MRI with fat saturation shows a **heterogeneous hypo- to isointense appearance of the metastasis** (arrow). (**c**) Axial T1 post-contrast MR with fat saturation shows **homogeneous enhancement of the metastasis** (arrow)

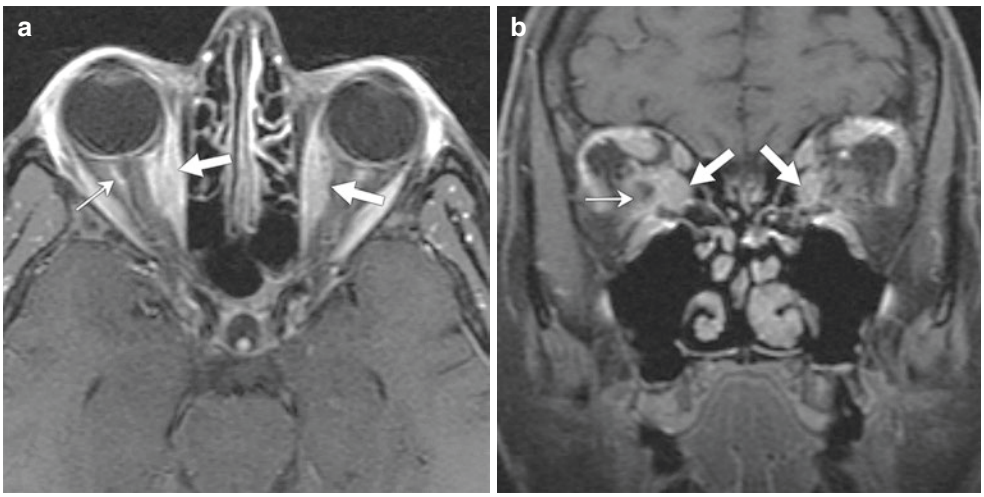

Fig. 4.19 A 23-year-old female with breast cancer who presented with orbital pain and diplopia. (**a**, **b**) Axial and coronal T1 post-contrast MRI with fat saturation show **metastases to bilateral medial rectus muscles** (arrows) **with intraconal disease in the right orbit surrounding the optic nerve** (thin arrows)

MRI

- The appearance **depends on the tumor type,** but metastases **tend to be T1 hypointense, T2 hyperintense with variable enhancement**.
- **T1 hyperintense lesions are from vascular metastasis such as renal or thyroid carcinoma, or melanoma** [61].

PET

- **^{18}F-FDG uptake depends on the FDG avidity of the primary tumor** [62].

Key Points

- List the **number of orbital lesions**.
- Describe the **orbital structures that are involved**, e.g., EOM, bone.
- Search for **other sites** of involvement, e.g., brain metastases, neck nodes.
- **Attempt to determine if the lesion is a metastasis versus a separate primary tumor.**

Graves' Eye Disease

Figures 4.20 and 4.21 show cases of thyroid eye disease.

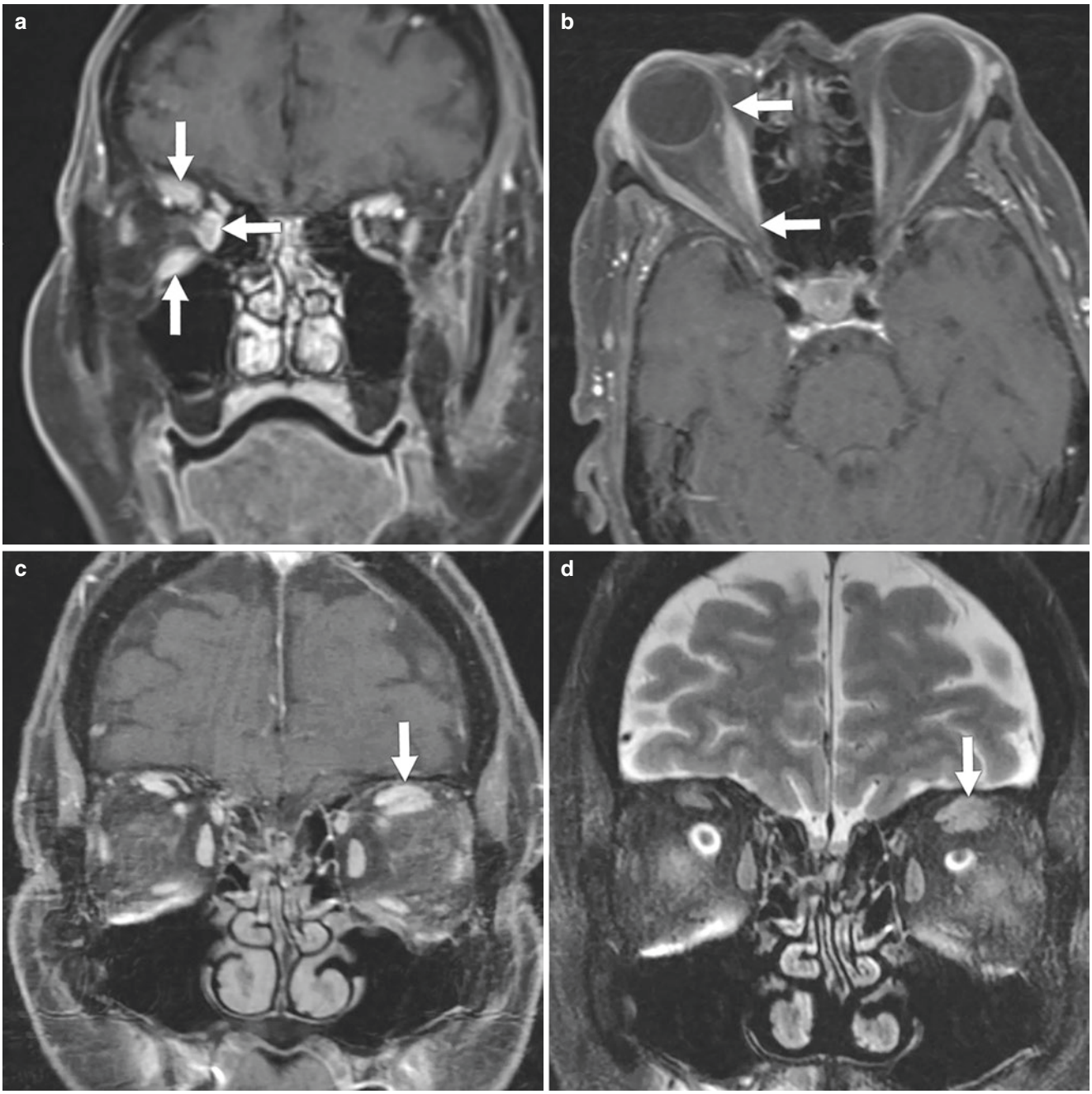

Fig. 4.20 (**a**, **b**) A 66-year-old female with a history of hyperthyroidism who presented with right eye exophthalmos and intermittent diplopia due to Graves' eye disease. (**a**) Coronal T1 post-contrast MRI with fat saturation shows enlargement with **enhancement of the right superior, medial, and inferior rectus muscles** (arrows). (**b**) Axial T1 post-contrast MRI with fat saturation shows **enlargement of the right medial rectus muscle that spares the tendinous insertions** (arrows). (**c**, **d**) A 43-year-old female with hyperthyroidism and Graves' eye disease. (**c**) Coronal T1 post-contrast MRI with fat saturation shows **enlargement of the left superior rectus-levator muscle complex** (arrow). (**d**) Coronal T2 MRI with fat saturation shows **enlargement and signal hyperintensity in the left superior rectus-levator muscle complex related to edema** (arrow)

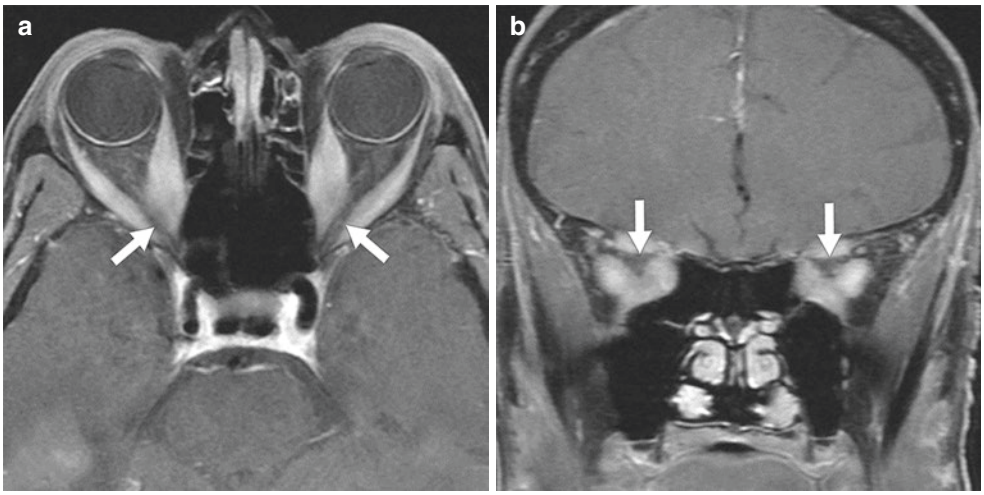

Fig. 4.21 A 30-year-old female with a history of hyperthyroidism and Graves' eye disease. (**a**, **b**) Axial and coronal T1 post-contrast MRI with fat saturation shows **enlargement of the EOMs with crowding at the orbital apex and compression upon the optic nerves** (arrows)

Background

- Graves' disease is an **autoimmune disorder**.
- **Graves' disease** is generally attributed to **genetic (79%)** or **environmental factors (21%)** [63]**.**
- Circulating anti-thyroid-stimulating hormone receptor autoantibodies bind to thyroid-stimulating hormone receptors, **stimulating the thyroid follicular cells to release T3 and T4**.
- **Increased T3 and T4 cause thyrotoxicosis with autoreactive lymphocyte deposition in the thyroid gland** [64].
- **Graves' eye disease (GED)**: an inflammatory condition affecting the orbital soft tissues.
  - Approximately 25% of patients with Graves' disease have GED [65, 66].

Presentation

- More common in **women**.
- Usually presents between **30 and 60 years of age** [67].
- **Symptoms of hyperthyroidism**: fatigue, weight loss, palpitations, anxiety, sleep disturbance, heat intolerance, and polydipsia [68, 69].
- **Upper eyelid retraction** occurs in greater than 80% of patients with GED.
  - Eyelid retraction may be recognized by others [70].

Imaging

- **Proptosis results from expansion of retro-orbital fat and/or EOMs**.
- **Compressive optic neuropathy (CON)**: serious but relatively infrequent complication.
  - Occurs in approximately 6% of patients [71].
  - May arise from **hypertrophied EOMs** compressing on the optic nerve at the orbital apex.
- **Bilateral orbital involvement in approximately 90% of patients** even if clinical manifestations appear unilateral or asymmetric [72].
- **Enlarged EOMs with sparing of the tendinous insertions** [72].
- **Signs of CON**: EOM crowding at the orbital apex and/or fat plane effacement around the optic nerve by enlarged EOMs [73–77] and optic nerve narrowing [78].

CT

- **Hypodensity of the EOMs** from lymphocyte accumulation and mucopolysaccharide deposition [72].
- **Increased orbital fat may lead to stretching of the optic nerve, eyelid edema, lacrimal gland prolapse, and bony orbit remodeling** [79].

MRI

- **Fatty infiltration of the EOMs appears T1 hyperintense.**
- **T2 hyperintensity of EOMs related to edema**.
- **Enlargement and enhancement of the EOMs** [80, 81].

Key Points

- Search for the presence or absence of **EOM tendon involvement**.

- **Describe involved muscles** (lateral rectus is rarely involved in isolation for GED).
- Search for signs of **optic nerve compression at the orbital apex** by enlarged extraocular muscles.

Idiopathic Orbital Inflammation

Figures 4.22 and 4.23 show cases of idiopathic orbital inflammation.

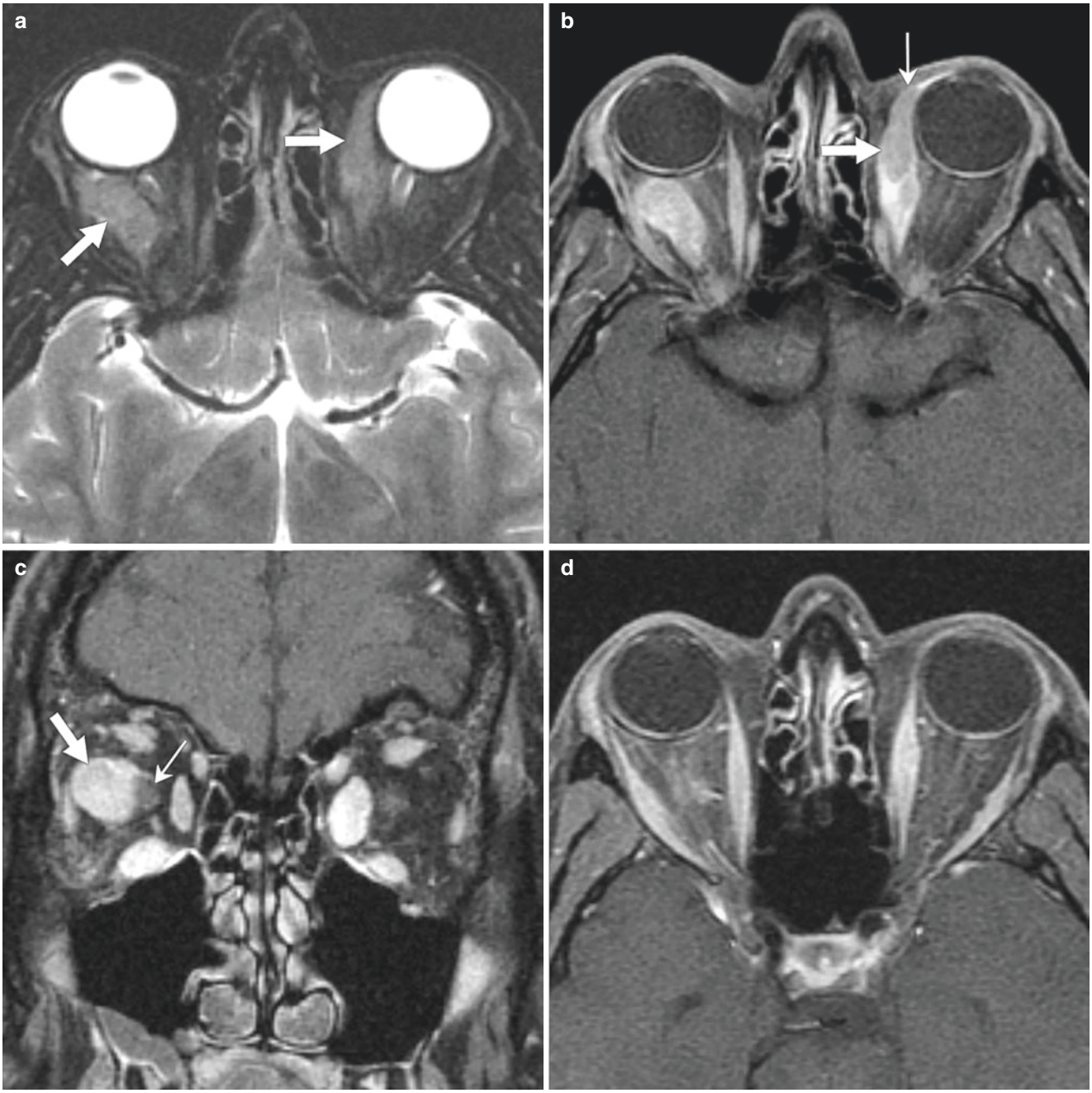

Fig. 4.22 A 35-year-old male with proptosis and periorbital edema due to idiopathic orbital inflammation. (**a**) Axial T2 MRI with fat saturation shows **isointense intraconal disease in the right orbit and an isointense mass involving the left medial rectus muscle** (arrows). (**b**) Axial T1 post-contrast MRI with fat saturation shows **enhancing disease in the left medial rectus muscle** (arrow) **with involvement of the tendinous insertion** (thin arrow). Note **enhancing disease in the right intraconal space**. (**c**) Coronal T1 post-contrast MRI with fat saturation show **enhancing disease in the right intraconal space** (arrow) **with abutment of the optic nerve** (thin arrow). The **left medial rectus muscle is also enlarged**. (**d**) Axial T1 post-contrast MRI with fat saturation shows **decreasing disease following treatment**

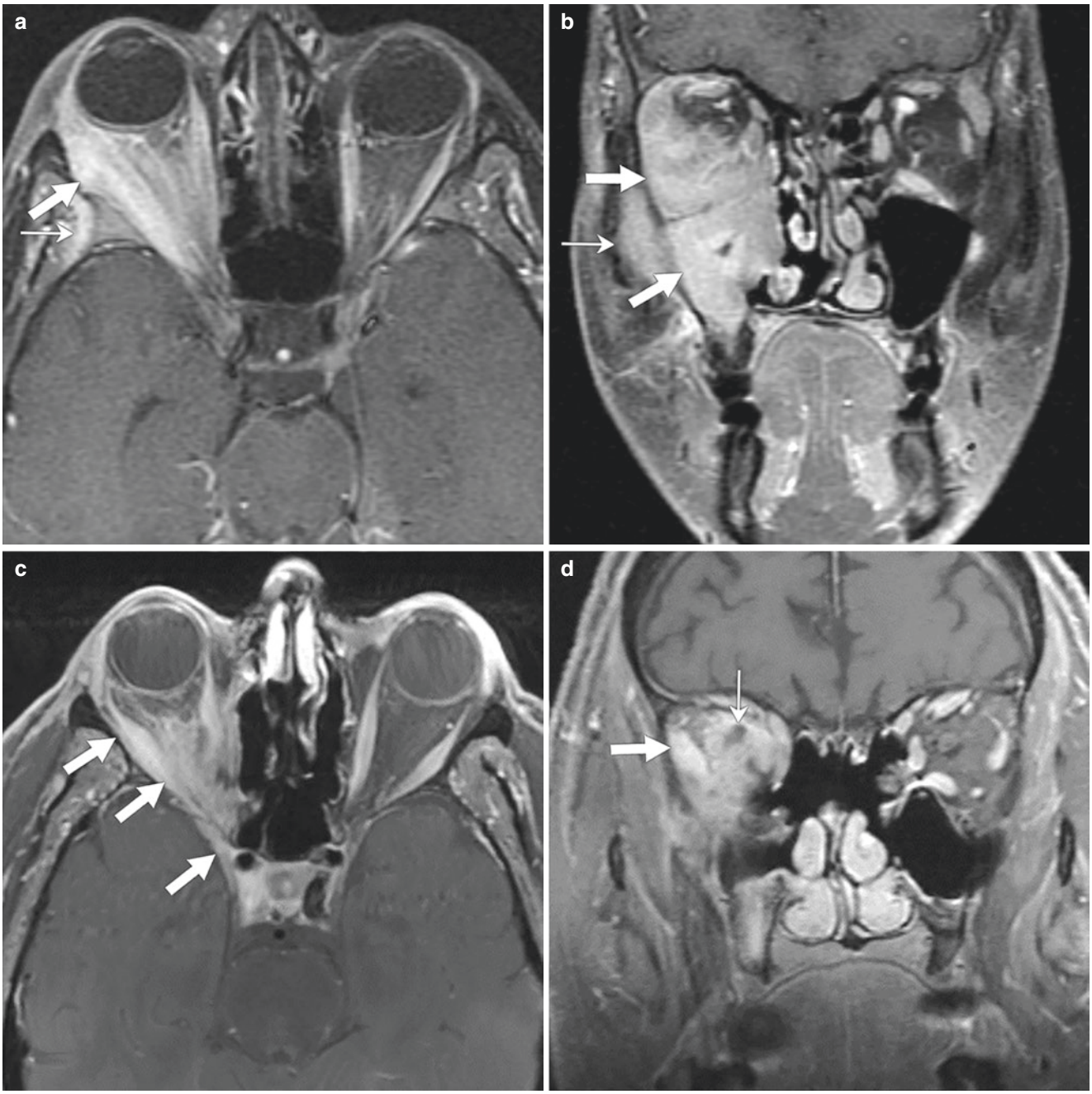

Fig. 4.23 (**a**, **b**) An 18-year-old male presented with gradual vision loss in the right eye due to idiopathic orbital inflammation (IOI) . (**a**) Axial T1 post-contrast MRI with fat saturation shows **disease in the right intraconal and extraconal spaces with involvement of the lateral rectus muscle** (arrows) and **right masticator space** (thin arrow). (**b**) Coronal T1 post-contrast MRI with fat saturation shows **disease in the right intraconal and extraconal spaces, involving the extraocular muscles, right maxillary sinus** (arrows), and the **right masticator space** (arrows). (**c**, **d**) A 63-year-old male with recurrent IOI. (**c**) Axial T1 post-contrast MRI with fat saturation shows **disease in the right lateral rectus muscle and intraconal space with posterior extension to the cavernous sinus** (arrows). (**d**) Coronal T1 post-contrast MRI with fat saturation shows **disease in the right lateral rectus muscle and intraconal space** (arrows) **that surrounds and elevates the optic nerve** (thin arrow)

Background

- **Idiopathic orbital inflammation (IOI)** was previously referred to as **orbital pseudotumor**.
- Inflammatory conditions characterized by **polymorphous lymphocyte infiltration and fibrosis of varying degrees** [82, 83].
- **Third most common disease affecting the orbit after GED and lymphoproliferative disorders** [84].
- **Tolosa–Hunt syndrome**: a rare subtype of IOI with involvement confined to the orbital apex and/or cavernous sinus, resulting in **acute orbital pain and paralysis of cranial nerves III, IV, and VI** [85].

Presentation

- **Symptoms**: headache, periorbital pain, and inflammatory signs including soft tissue swelling and erythema.
- **Compression upon the orbital apex and cavernous sinus involvement** may lead to decreased visual acuity and cranial nerve palsies [86].

Imaging

- **Nonspecific inflammatory soft tissue** is present in the orbit with infiltration of the orbital fat.
- When the EOMs are involved, IOI **may include the tendinous portion of the muscles.**
- Other sites of involvement include the **lacrimal gland, optic nerve including the junction with the globe, and adjacent periorbital soft tissues**.
- **Retro-orbital involvement** may occur from extension through the superior and inferior orbital fissures and the optic canal with involvement of the cavernous sinus [82].

CT

- **Enhancement with contrast** [85].

MRI

- IOI is **T1 isointense** and **T2 iso- to hypointense** which may be due to fibrosis.
- **Variable contrast enhancement** [86, 87].
- Restricted diffusion has been described [88].

Key Points

- Search for the presence or absence of **EOM tendon involvement**.
- **Determine which muscles are involved** (lateral rectus is rarely involved in isolation for GED).
- Search for **involvement of the orbital apex and/or cavernous sinus**.

Immunoglobulin G4-Related Disease

Figures 4.24 and 4.25 show cases of IgG4-related disease.

Background

- **Immunoglobulin G4-related disease (IgG4-RD)** is a **systemic disease of unknown etiology**.
- Characterized by **inflammation, fibrosis, and tissue infiltration with plasma cells that express IgG4.**
- **Various organs may be involved**, including the pancreas, bile duct, liver, retroperitoneal soft tissues, lung, thyroid, salivary glands, and lymph nodes either alone or systematically [89, 90].
- **After the pancreas, the head and neck region is the second most affected site** [91].

Presentation

- **Symptoms of IgG4-RD** include hypophysitis, thyroiditis, pancreatitis, cholecystitis, retroperitoneal fibrosis, and lymphadenopathy [91–95].
- Occurs predominantly in **older men**.
- Frequently associated with **elevated serum IgG4 levels** [92, 96].
- Can involve the **orbit including the EOMs and optic nerve**.
- **Other sites of disease in the head and neck**: pituitary gland, cavernous sinus, paranasal sinuses, and cervical nodes [91].
- **Lacrimal involvement (dacryoadenitis)** may occur in isolation or with salivary gland involvement (sialadenitis) as part of **Mikulicz's disease** (painless bilateral enlargement of the lacrimal, parotid, and submandibular glands) [94].

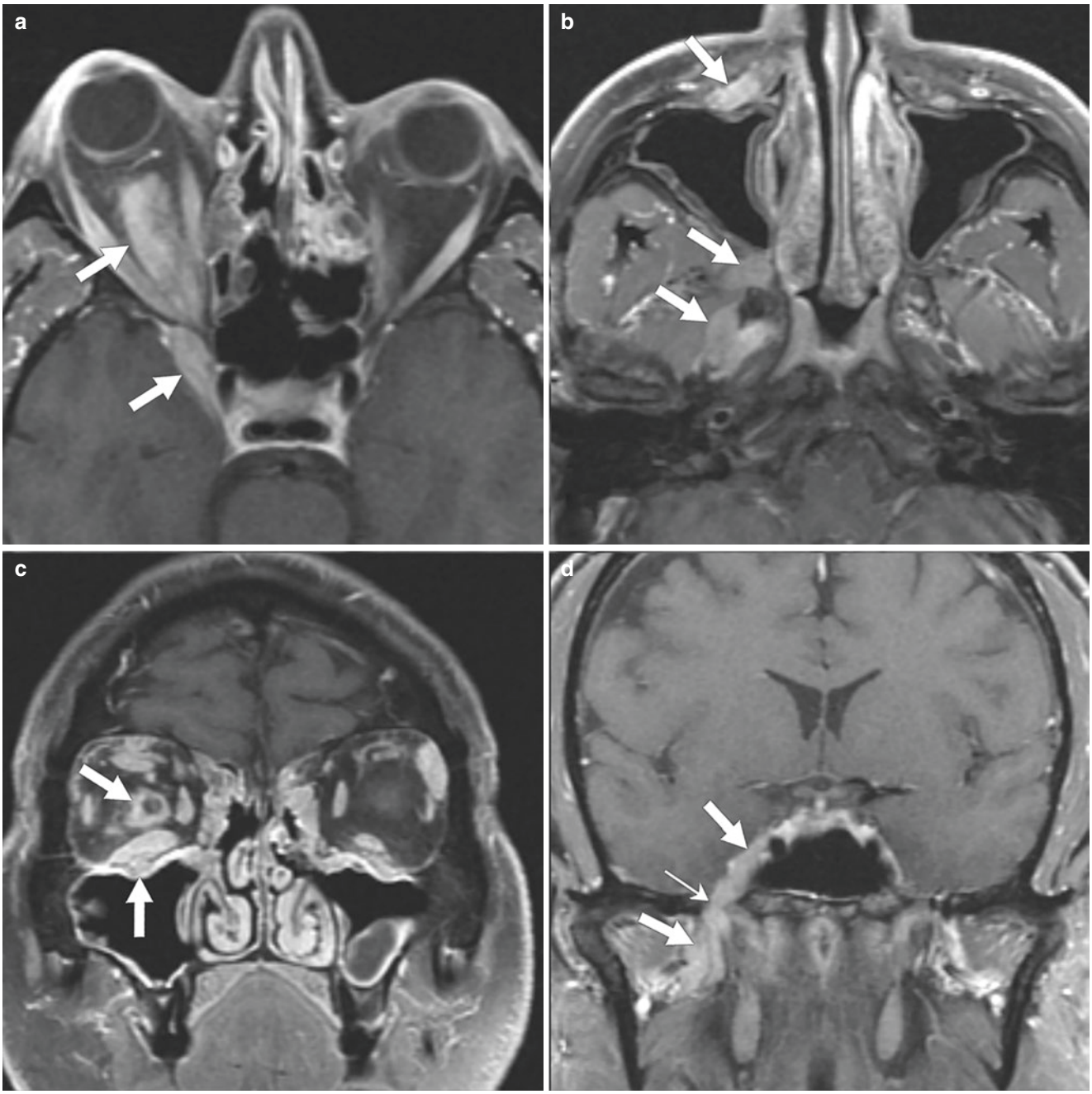

Fig. 4.24 A 43-year-old male with right lacrimal swelling due to IgG4-RD. (**a**) Axial T1 post-contrast MRI with fat saturation shows **infiltrative disease involving the right inferior rectus muscle with posterior spread of disease to the right cavernous sinus** (arrows). (**b**) Axial T1 post-contrast MRI with fat saturation shows **disease in the right premaxillary soft tissues, pterygopalatine fossa, right masticator space, and foramen ovale** (arrows). (**c**) Coronal T1 post-contrast MRI with fat saturation shows **disease surrounding the right optic nerve and involving the right infraorbital nerve (V_2)** (arrows) and the **superior rectus-levator muscle complex**. (**d**) Coronal T1 post-contrast MRI with fat saturation shows **disease involving the right mandibular nerve (V_3)** (arrows) **as it extends through the foramen ovale** (thin arrow)

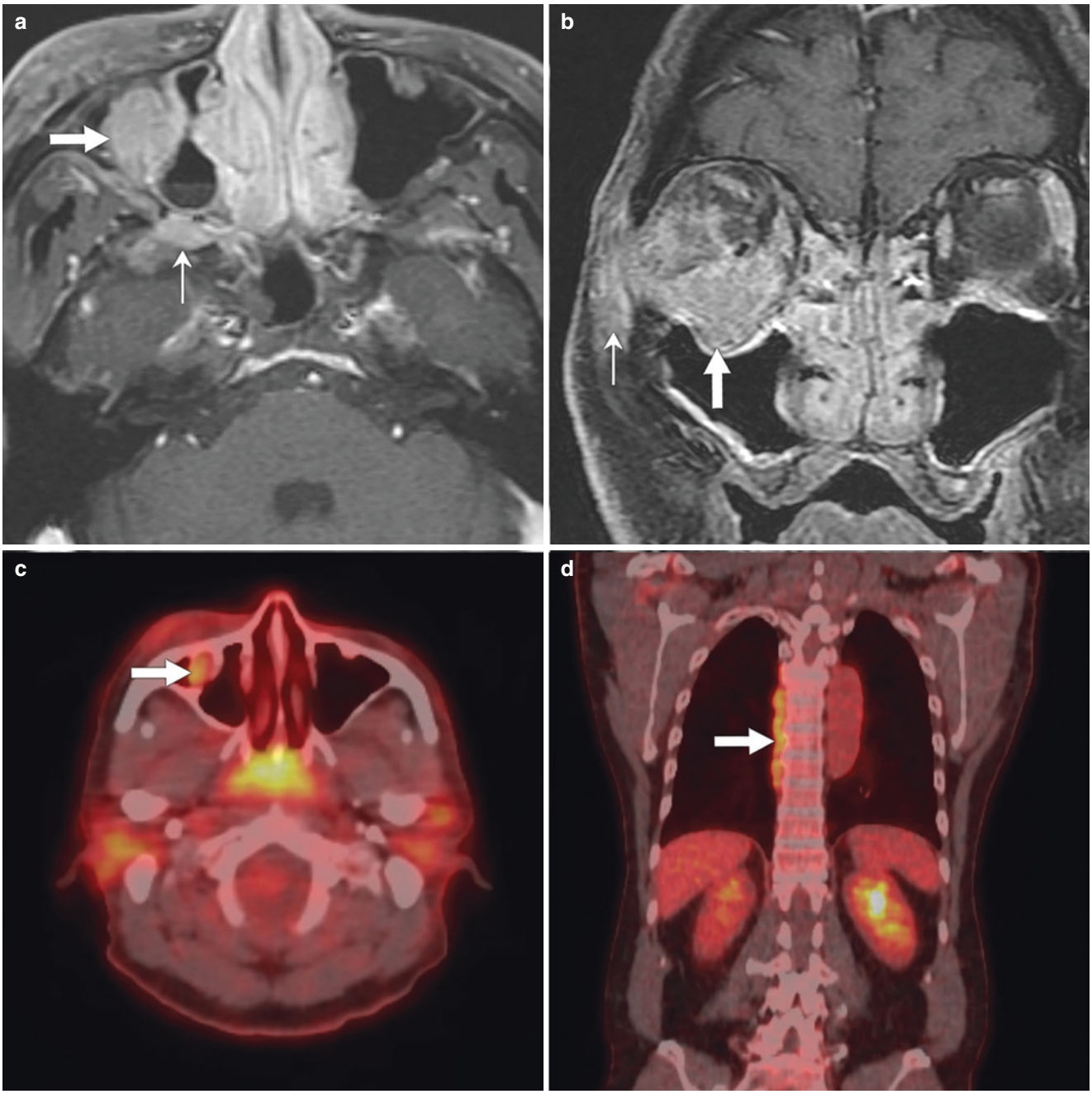

Fig. 4.25 A 60-year-old male with right lacrimal swelling due to IgG4-RD. (**a**) Axial T1 post-contrast MRI with fat saturation shows **disease in the inferior right orbit** (arrow) and the **right pterygopalatine fossa** (thin arrow). (**b**) Coronal T1 post-contrast MRI with fat saturation shows **disease in the inferior right orbit with involvement of the right infraorbital nerve (V_2)** (arrow) **and right face** (thin arrow). (**c**) Axial ^{18}F-FDG PET/CT shows **FDG avidity in the right infraorbital nerve (V_2)** (arrow). (**d**) Coronal ^{18}F-FDG PET/CT shows **FDG-avid disease along the right side of the thoracic vertebral bodies** (arrows)

Imaging

- The **most common sites are the lacrimal gland and EOMs**, which are affected in most patients with this diagnosis [96].
- The **lacrimal glands are enlarged, which may be unilateral or bilateral**.
- **Other possible findings about the orbits** include enlargement of the EOMs, infiltration of the orbital fat, cranial nerve involvement especially the infraorbital nerve (V_2), and soft tissue in the cavernous sinuses and Meckel's caves [96].
- Associated **paranasal sinus inflammatory mucosal thickening** has been reported [96].

CT

- **Homogeneous** soft tissue with **contrast enhancement**.

MRI

- **T1 hypointensity, T2 hypo- to hyperintensity** with **homogeneous enhancement** [92, 95].

PET

- IgG4-RD cases are ^{18}**F-FDG-avid** and PET/CT is useful to detect multi-organ involvement, guide biopsies, and assess treatment response [92, 97].

Key Points

- Search for **involvement of the salivary glands,** e.g., parotid, submandibular glands.
- Search for **involvement of cranial nerves,** e.g., infraorbital nerve, cavernous sinus, and Meckel's cave.
- Search for o**ther sites of disease involvement throughout the body**.

Sarcoidosis

Figures 4.26 and 4.27 show cases of sarcoidosis in the orbit.

Background

- Chronic systemic multiorgan disorder characterized by a **non-caseating granulomatous reaction**.
- Unknown etiology.
- **Can affect nearly every organ in the body,** with **orbital involvement reported in 25–83%** of the patients [98, 99].
- The **lungs, skin, orbits, and lymph nodes** are most commonly affected; however, the liver, kidneys, heart, and brain may also be involved [98, 99].
- **Biopsy is often required** and demonstrates the non-caseating granulomas [4].

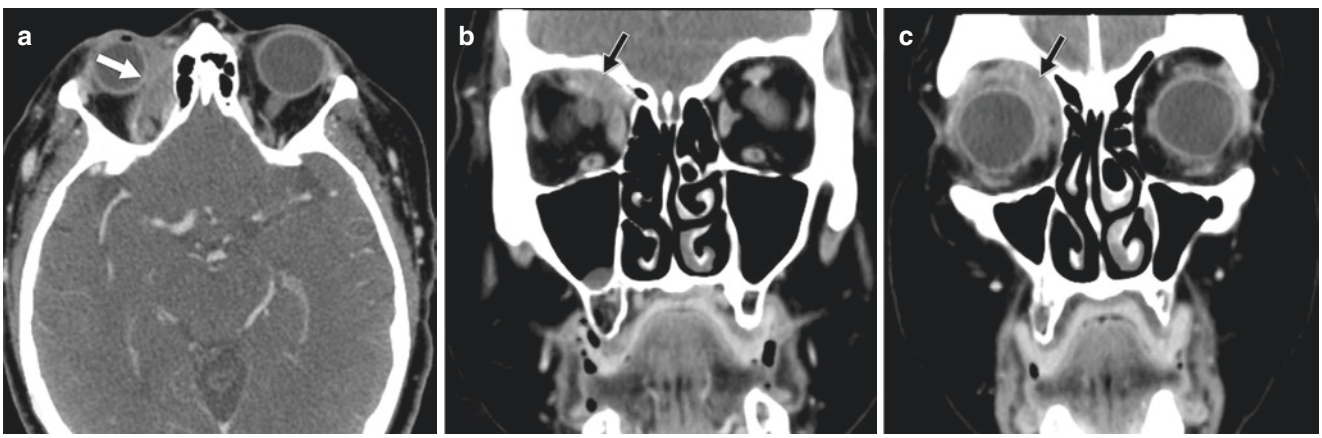

Fig. 4.26 A 60-year-old female being treated for sarcoidosis presented with fullness in the right upper eyelid. (**a**, **b**) Axial and coronal CT with contrast, soft tissue window shows **disease in the superonasal right orbit** (arrows). (**c**) Coronal CT with contrast, soft tissue window shows **anterior extension of disease superior and medial to the right globe** (arrow) with **inferolateral displacement of the globe**

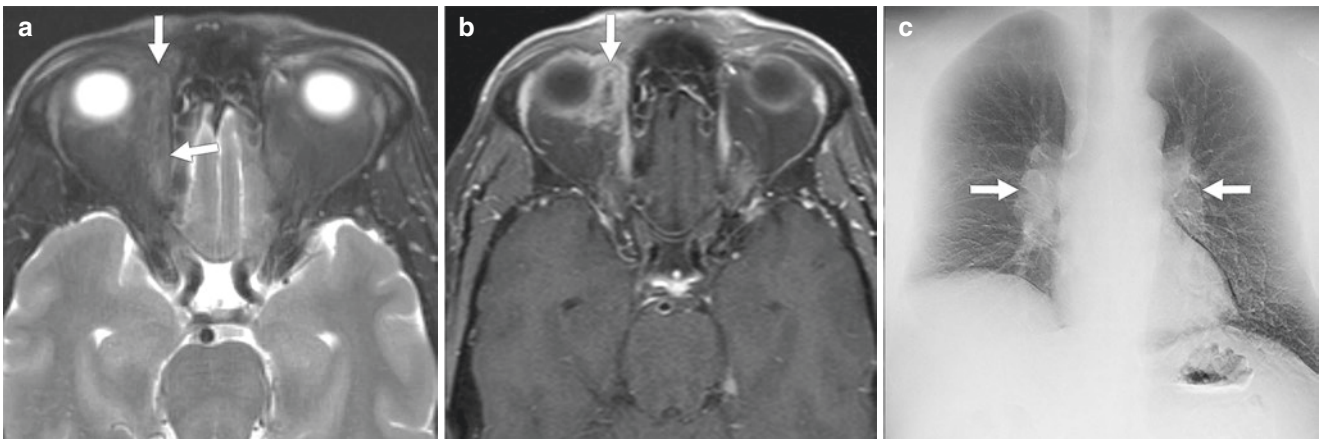

Fig. 4.27 A 57-year-old male presented with right eye swelling and diplopia due to sarcoidosis. (**a**) Axial T2 MRI with fat saturation shows **hypointense disease in the pre- and postseptal superonasal right orbit** (arrow). (**b**) Axial T1 post-contrast MRI with fat saturation shows **heterogeneous enhancement of the disease** (arrow). (**c**) Plain chest radiograph shows **bilateral hilar adenopathy** (arrows)

Presentation

- Primarily develops in patients aged **25–45 years old**, although children and older individuals may also be affected [100].
- **Ocular involvement in 20% of patients** [101].
- **African Americans** have a higher incidence of ocular involvement compared to Whites [102].
- Manifestations include **anterior uveitis** followed by **posterior uveitis** which can severely impact visual acuity [103].
- The **cranial nerves, leptomeninges, brain parenchyma, and hypothalamic-pituitary axis** may also be involved. **Diabetes insipidus may result** [100].
- The **parotid gland** is involved in 5% of cases [101].
- **Other findings** include enlarged hilar lymph nodes, pulmonary infiltrates, and skin disease.
- High serum **angiotensin-converting enzyme level** is present but not specific [104].

Imaging

- Can involve the **orbital fat, EOMs, optic nerve sheath, and lacrimal gland** [105].
- **Displacement of the globe** including **proptosis** may be present [106].

CT

- **Homogeneous enhancement** [105].

MRI

- **EOM involvement** is characterized by **abnormal thickening and enhancement of the muscles and tendinous insertions**.
- **Infiltrative and enhancing soft tissue can be seen in the retrobulbar fat** [107].
- The **optic nerves** may show **thickened enhancing nodules with T2 signal hyperintensity of the nerve**.
- **Diffusely enlarged and enhancing lacrimal glands** [108].

Nuclear Medicine

- **PET/CT and Gallium scans** aid in diagnosis when orbital, parotid and bilateral hilar uptake is detected [107].

Key Points

- Search for other sites of involvement throughout the body (e.g., regional lymph nodes).

Granulomatosis with Polyangiitis

Figures 4.28 shows a case of granulomatosis with polyangiitis.

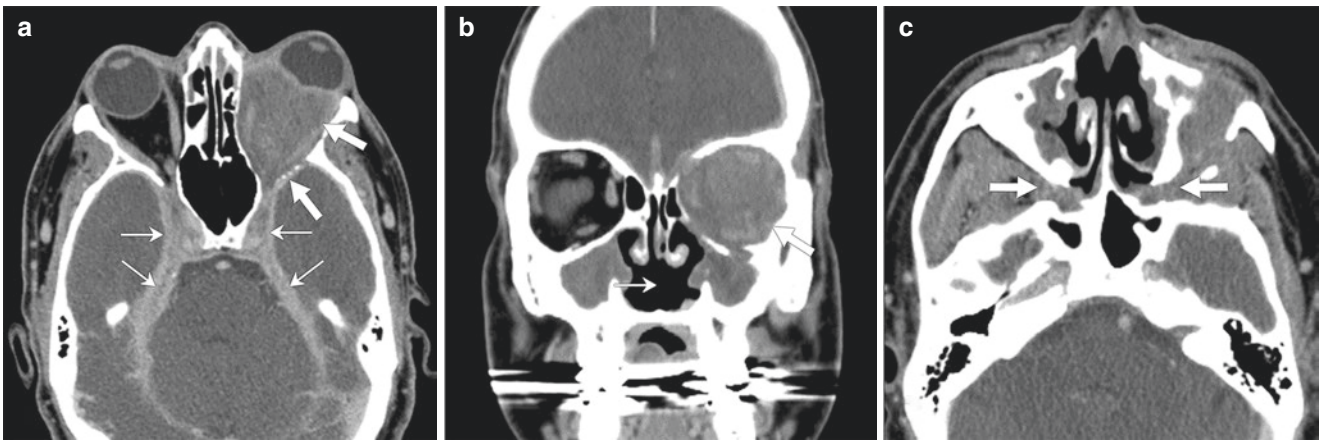

Fig. 4.28 A 37-year-old male with granulomatosis with polyangiitis who presented with left orbital pain. (**a**) Axial CT with contrast, soft tissue window shows a **heterogeneously enhancing soft tissue in the left orbit with compression upon a proptotic globe and destruction of the sphenoid bone** (arrows). **Disease extends posteriorly to involve bilateral cavernous sinuses, Meckel's caves, and the tentorium** (thin arrows). (**b**) Coronal CT with contrast, soft tissue window shows the **intraconal and extraconal inflammatory soft tissue in the left orbit** (arrow). Note **changes in the sinonasal cavity,** including **perforation of the nasal septum** (thin arrow) and **destruction of the medial walls of the maxillary sinuses**. (**c**) Axial CT with contrast, soft tissue window shows **disease in the pterygopalatine fossae** (arrows)

Background

- **Granulomatosis with polyangiitis** is an **idiopathic autoimmune disease leading to necrotizing granulomatous vasculitis** [109].
- **Previously named Wegener's granulomatosis**.
- **Antibodies to neutrophil cytoplasmic antigens (ANCA)** are present in approximately 80–90% of patients [110].
- **Tissue necrosis with vasculitis of small to medium vessels**.
- Characteristically presents with disease in the **nasal cavity, lungs, and kidney** [111].

Presentation

- The average age at presentation is **40–55 years, with no gender differences** [111].
- The **main presenting symptoms** are usually related to the **upper respiratory tract and renal and nasal cavity disease** [112].
- **Other symptoms**: diplopia, epistaxis, septal perforation, chronic sinusitis, chest pain, and hemoptysis.
- **Small vessel vasculitis causes symptoms such as conjunctivitis, scleritis, uveitis, retinitis, and optic neuritis**.
- **The orbits are involved in up to 58% of patients; ocular manifestations are non-specific** [110, 112].
- Granulomatous disease can lead to an **orbital inflammatory mass often with proptosis and optic nerve compression**.
- Severe orbital disease can cause **optic nerve compression and blindness** [113].
- A granulomatous pseudotumor involving the cranial nerves of the cavernous sinus **may present as Tolosa–Hunt syndrome** with painful ophthalmoplegia (weakness and paralysis of EOMs) [114].

Imaging

- Commonly presents as an **inflammatory infiltrate that molds around the orbital contour and may involve the adjacent paranasal sinuses** [115].
- Growth of the inflammatory infiltrate leads to the **formation of an orbital mass** [116].
- When the **sinonasal cavity** is involved, imaging findings include **mucosal thickening, bone erosion, and destruction** [117].

CT

- CT demonstrates **cartilage and bone destruction with nasal septum perforation, diffuse swelling of EOMs, and orbital inflammatory pseudotumor**.
- **Slightly hyperdense** to nasal mucosa on contrast-enhanced studies [112].

MRI

- In the **early stages of disease, mucosal inflammation and granulation tissue may have a similar appearance**.
- In **later stages**, the disease appears **slightly T1 hypointense, T2 hyperintense with homogeneous enhancement**.
- **Contour may be indistinct** [109].

Key Points

- Search for the presence of **scleritis** or **optic neuritis**.
- Search for the involvement of the **nasal cavity/paranasal sinuses and bone destruction**.

Waldenstrom Macroglobulinemia

Figure 4.29 shows a case of Waldenstrom macroglobulinemia.

Background

- **Waldenstrom macroglobulinemia** is a type of **non-Hodgkin lymphoma also named "lymphoplasmacytic lymphoma"** [118, 119].
- **Mature B-cell neoplasm** with small lymphocytes showing "plasmacytoid–plasma cell differentiation in the absence of features of other lymphoproliferative disorders" [119, 120].
- **Waldenstrom macroglobulinemia is diagnosed with bone marrow involvement of IgM-producing lymphoplasmacytic lymphoma**.
- **Multisystem disease process that can affect any organ with a variety of manifestations** [118, 119].

Presentation

- Median age at diagnosis is **70 years old**.
- Higher occurrence rate in **men and Whites** [121, 122].
- **Bing–Neel syndrome (BNS)** represents CNS involvement of Waldenstrom macroglobulinemia with neoplastic cells [123–125].

Imaging

- **CNS disease**: brain parenchyma, dura, leptomeninges, cranial nerves (mainly the optic nerve), and spinal cord [123–125].
- **Two categories of CNS involvement: diffuse form and tumoral form.**
  - May be unifocal or multifocal [126].
- **Retro-orbital collections** of lymphoplasmacytoid cells can cause reduced motility and proptosis [127].
- **Lacrimal gland, conjunctival, and vitreous involvement** have also been reported [128].

MRI

- Lesions in the diffuse form are reported to **be T1 hypointense and T2 hyperintense**.
- In the brain parenchyma, "**ring-shaped or nodular enhancement, with or without surrounding edema**" has been reported [124].
- **Thickened enhancement of the cranial nerves, meninges, and spinal nerve roots** [124].

PET/CT

- Bing–Neel syndrome has been reported to be ^{18}F-FDG avid [129].

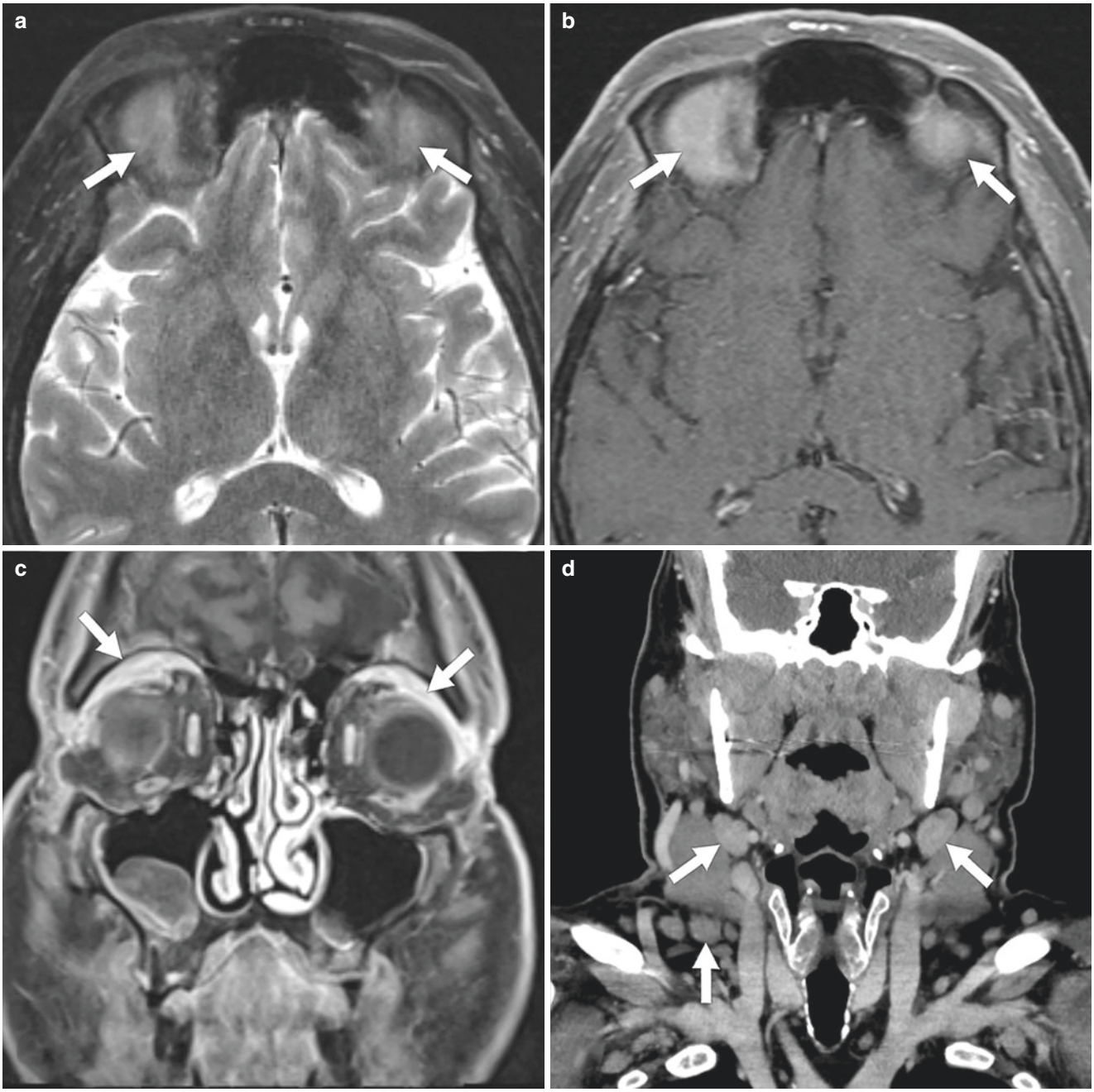

Fig. 4.29 A 59-year-old male presented with intermittent blurry vision and was later diagnosed with Waldenstrom macroglobulinemia. (**a**) Axial T2 MRI with fat saturation shows **isointense lesions in the superior orbits** (arrows). (**b**, **c**) Axial and coronal T1 post-contrast MRI with fat saturation shows **homogeneous enhancement of lesions in bilateral superotemporal orbits** (arrows). (**d**) Coronal CT with contrast, soft tissue window shows **extensive bilateral cervical adenopathy** (arrows)

Amyloidosis

Figures 4.30 and 4.31 show cases of amyloidosis.

Background

- Amyloidosis is a disease of unknown etiology characterized by the **deposition of a proteinaceous amyloid protein** in tissues and organs.
- Amyloid may be **localized or systemic** and can accumulate in all the body's tissues [130, 131].
- **Often diagnosed by tissue biopsy**.
- Samples undergo **Congo red staining** and are viewed with a polarized light where amyloid has an **affinity for the Congo red and green birefringence** [132].

Presentation

- Typically affects **middle-aged** patients [133].
- Deposition of amyloid can occur in multiple ocular sites, including the **orbit, orbital adnexa, EOMs, lacrimal gland, eyelid, and conjunctiva.**
- **Symptoms**: eyelid swelling, discomfort, proptosis, hyperemia of the bulbar conjunctiva, subconjunctival hemorrhage, and lacrimal gland enlargement [132].

Imaging

- **CT may be more informative than MRI in differentiating periocular and orbital amyloidosis** owing to the higher sensitivity of detecting **calcifications and bony changes**.
- With orbital involvement, the **mass may mold to the globe but can cause displacement**.
- **EOM enlargement** may also be present [134, 135].

CT

- On CT, amyloid may appear as a **homogeneous, slightly hyperdense soft tissue mass that may show calcifications**.
- **Erosion of the orbital wall** has been reported [134, 135].

MRI

- **T2 hypointense** with **heterogeneous contrast enhancement** [130, 131].

PET

- May be ^{18}F-FDG-avid.

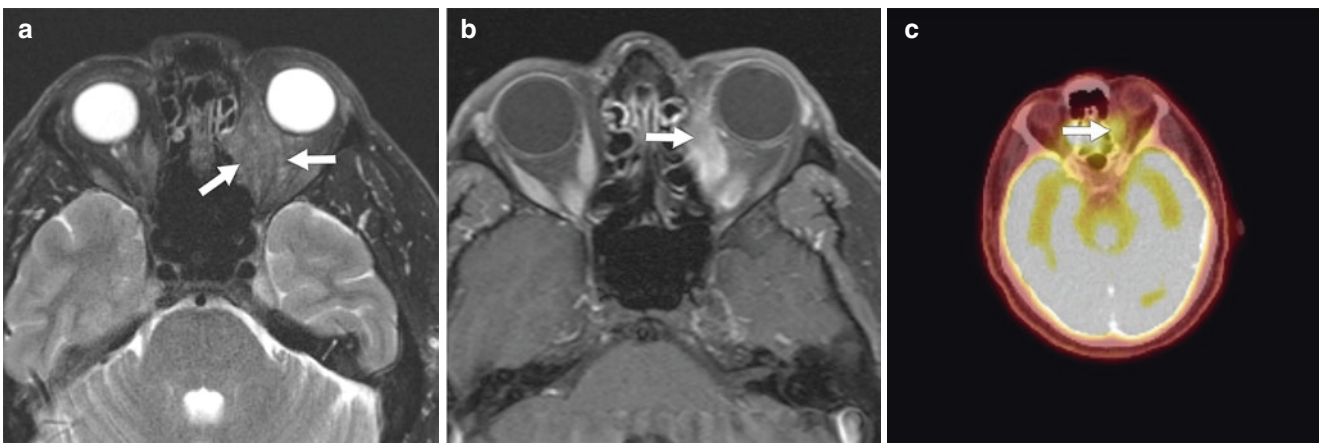

Fig. 4.30 A 55-year-old male was referred after biopsy of a left orbital mass demonstrating amyloidosis. (**a**) Axial T2 MRI with fat saturation shows **hypointense disease in the medial left orbit and ethmoid air cells** (arrows). (**b**) Axial T1 post-contrast MRI with fat saturation shows **heterogeneous enhancement of the disease** (arrows). (**c**) Axial ^{18}F-FDG PET/CT shows **FDG avidity of the disease in the medial left orbit**

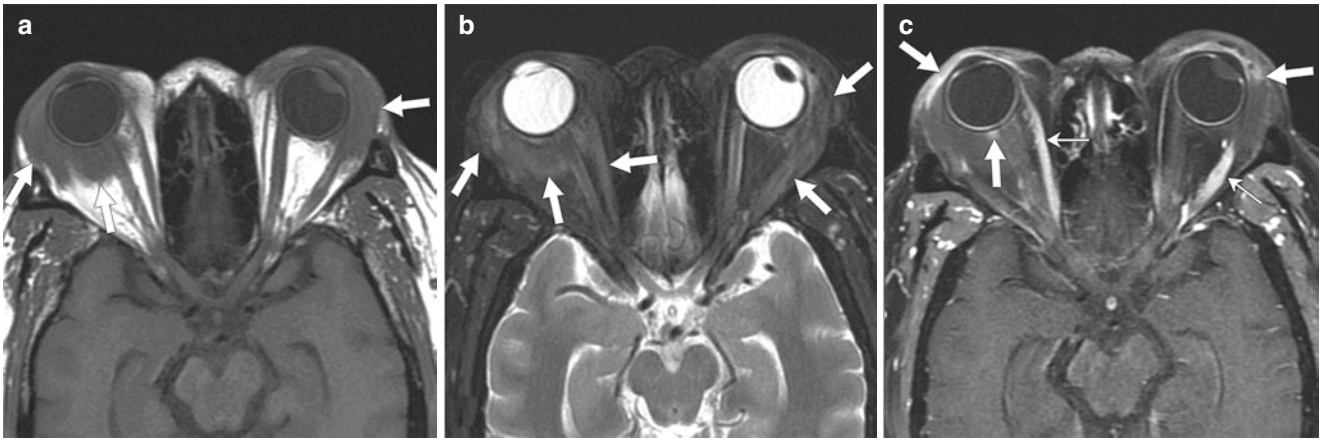

Fig. 4.31 A 64-year-old female who presented with pain and periorbital amyloidosis. (**a**) Axial non-contrast MRI without fat saturation shows **isointense disease in the pre- and postseptal orbits, including the right intraconal space** (arrows). (**b**) Axial T2 MRI with fat saturation shows a **hypointense appearance of amyloidosis** (arrows). (**c**) Axial T1 post-contrast MRI with fat saturation shows a **small degree of enhancement of the disease** (arrows) **except in the right medial and left lateral rectus muscles that demonstrate enhancement** (thin arrows)

Erdheim–Chester Disease

Figure 4.32 shows a case of Erdheim–Chester disease.

Background

- **Non-Langerhans cell histiocytosis** characterized by **multi-organ disease involvement**.
- **Specific immunohistochemical profile**: histiocytes stain positive for CD68, negative for CD1a, and positive or negative for S100 [136].

Presentation

- **Average age at diagnosis: 53 years**; slight male predominance [136, 137].
- **Multiple systemic manifestations** including the CNS and cardiovascular, pulmonary, and musculoskeletal systems.
- **Predilection for appendicular skeleton** [138].
- The **hypothalamic-pituitary axis** is the most common site in the CNS [139].
- **Variable clinical course**: some patients asymptomatic, and others succumb following rapid disease progression [140].
- **Symptoms**: exophthalmos, bone pain, diabetes insipidus, cerebellar or pyramidal symptoms, cardiac dysfunction, and renal impairment [141].

Imaging

- **Retro-bulbar masses** may develop secondary to histiocyte infiltration [140, 141].
- **Meningeal thickening** may mimic meningiomas.
- **Vertebral involvement** [140].
- **Bony medullary sclerosis** [139].

MRI

- Intraconal lesions are **T1 and T2 hypointense and enhance** [140, 141].

Key Points

- Search for other sites of disease, including the brain and pituitary gland, heart, lungs, and bones.

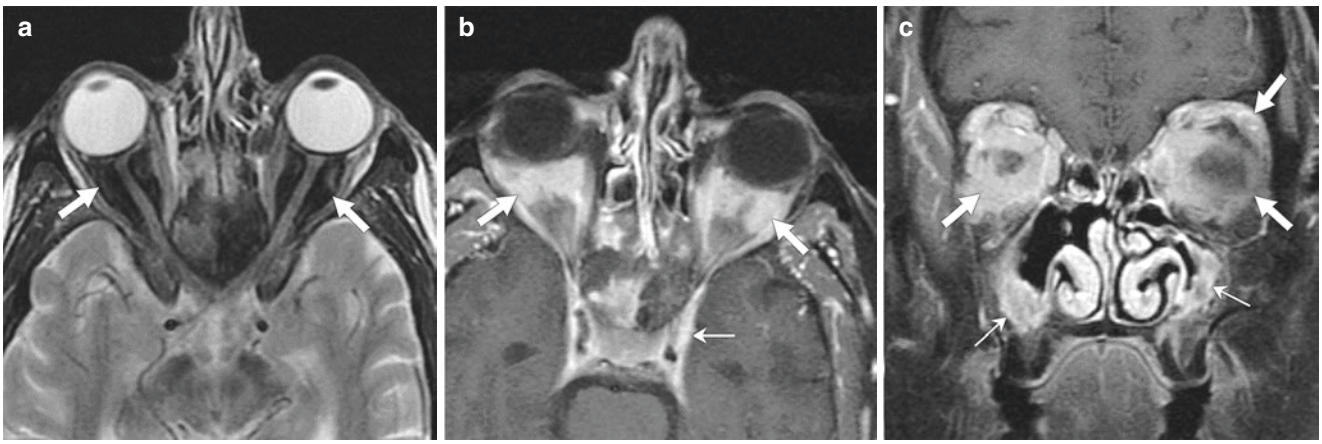

Fig. 4.32 A 61-year-old male with Erdheim-Chester disease who presented with orbital pain and blurry vision. (**a**) Axial T2 MRI without fat saturation shows **hypointense intraconal disease in bilateral orbits** (arrows). (**b**) Axial T1 post-contrast MRI with fat saturation shows **heterogeneous enhancement of the intraconal disease** (arrows) with **involvement of the left cavernous sinus** (thin arrow). (**c**) Coronal T1 post-contrast MRI with fat saturation shows **enhancing bilateral intraconal and extraconal disease** (arrows), and **enhancing disease in the maxillary sinuses** (thin arrows)

Infection

Figure 4.33 shows cases of orbital infection.

Background

- Orbital infections account for **greater than half of all primary orbital abnormalities**.
- Approximately two-thirds related to **sinusitis** and one-fourth result from **intraorbital foreign bodies** [142].

Presentation

- **Orbital abscess** is a serious complication of orbital cellulitis.
- A **subperiosteal abscess may develop from acute sinusitis involving the ethmoid air cells** [143].

Imaging

- **Preseptal cellulitis** characterized by swelling and stranding of the periorbital soft tissues anterior to the orbital septum [144].
- **Orbital cellulitis** demonstrates stranding of the soft tissues posterior to the orbital septum with clinical signs including proptosis, vision loss, and painful ophthalmoplegia.
- A **subperiosteal abscess** appears as a **peripherally enhancing fluid collection with a lenticular shape along the orbital wall** that **can laterally displace the medial rectus muscle** [142].

CT

- An orbital abscess appears as a **peripherally enhancing fluid collection in the orbit**. Adjacent soft-tissue standing and EOM involvement [142].

MRI

- An orbital abscess appears as a **peripherally enhancing fluid collection** with **restricted diffusion centrally on DWI** [142].

Key Points

- Search for **preseptal versus postseptal involvement**.
- Describe the **presence, size, and location** of an abscess.
- Assess for **signs of sinusitis**.

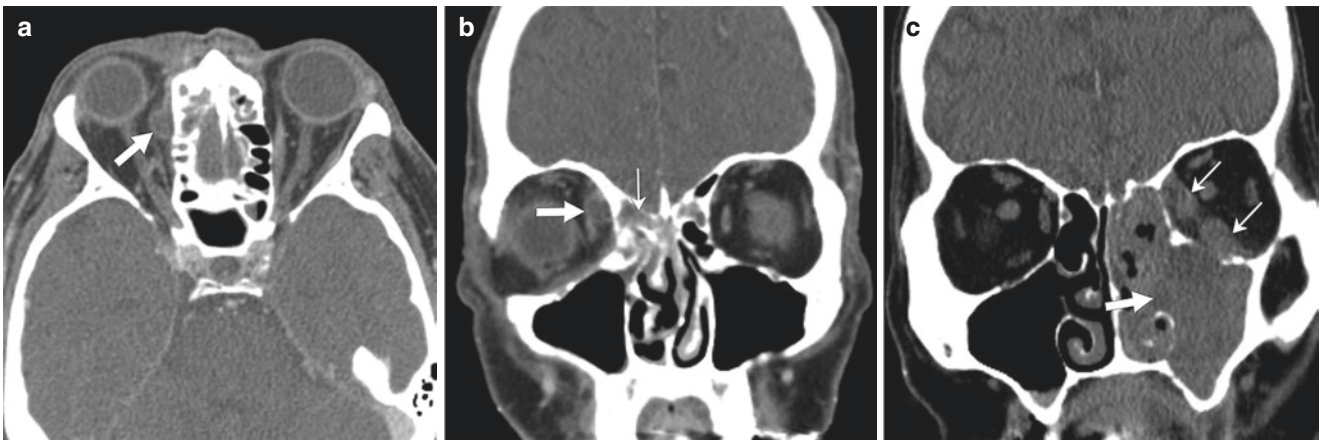

Fig. 4.33 (**a**, **b**) A 64-year-old female with COVID-19 infection, invasive fungal sinusitis, and a right orbital abscess. (**a**) Axial CT with contrast, soft tissue window shows **a peripherally enhancing abscess in the medial right orbit** (arrow). (**b**) Coronal CT with contrast, soft tissue window shows the **abscess with lateral displacement of the medial rectus muscle** (arrow) and **infection in the adjacent ethmoid air cells** (thin arrow). (**c**) An 81-year-old male with aplastic anemia and left maxillary fungal sinusitis. (**c**) Coronal CT without contrast, soft tissue window shows **inflammatory disease in the left maxillary sinus** (arrow) **with invasion of the left orbit and enlargement of the medial and inferior rectus muscles** (thin arrows)

Venous Malformation

Figures 4.34 and 4.35 show cases of orbital venous malformations.

Background

- **Venous malformations (cavernous hemangiomas) represent the most common vascular lesion in adults**.
- These lesions have a fibrous capsule surrounding endothelial-lined spaces and demonstrate **slow progressive enlargement** over time 145].
- Do not involute [145].
- **Slow flow vascular malformation** [4].

Presentation

- More common in **women**, often **detected in the second to fourth decades** [4].
- Usually solitary and **most often arise in the intraconal space** [145].
- **Often an incidental finding** during imaging for clinical symptoms such as headache, pain, proptosis, diplopia, palpable mass, and vision changes [146].

Imaging

- **Well-circumscribed, rounded intraconal lesions**.
- Due to a **slow-flow arterial supply**, contrast **does not fill the lesion entirely until the late venous phase**.
- **Bone remodeling and intralesional microcalcifications may occur** [145].

CT

- **Hyperdense on non-contrast CT**.
- May displace adjacent structures without invasion.
- **Contrast does not completely fill the lesion until the late venous phase** [4, 145].
- **Phleboliths** may be present [4].

MRI

- **T1 isointense and T2 hyperintense**.
- In larger lesions, **internal septa** may be visualized.
- **Contrast does not completely fill the lesion entirely until the late venous phase** [145].

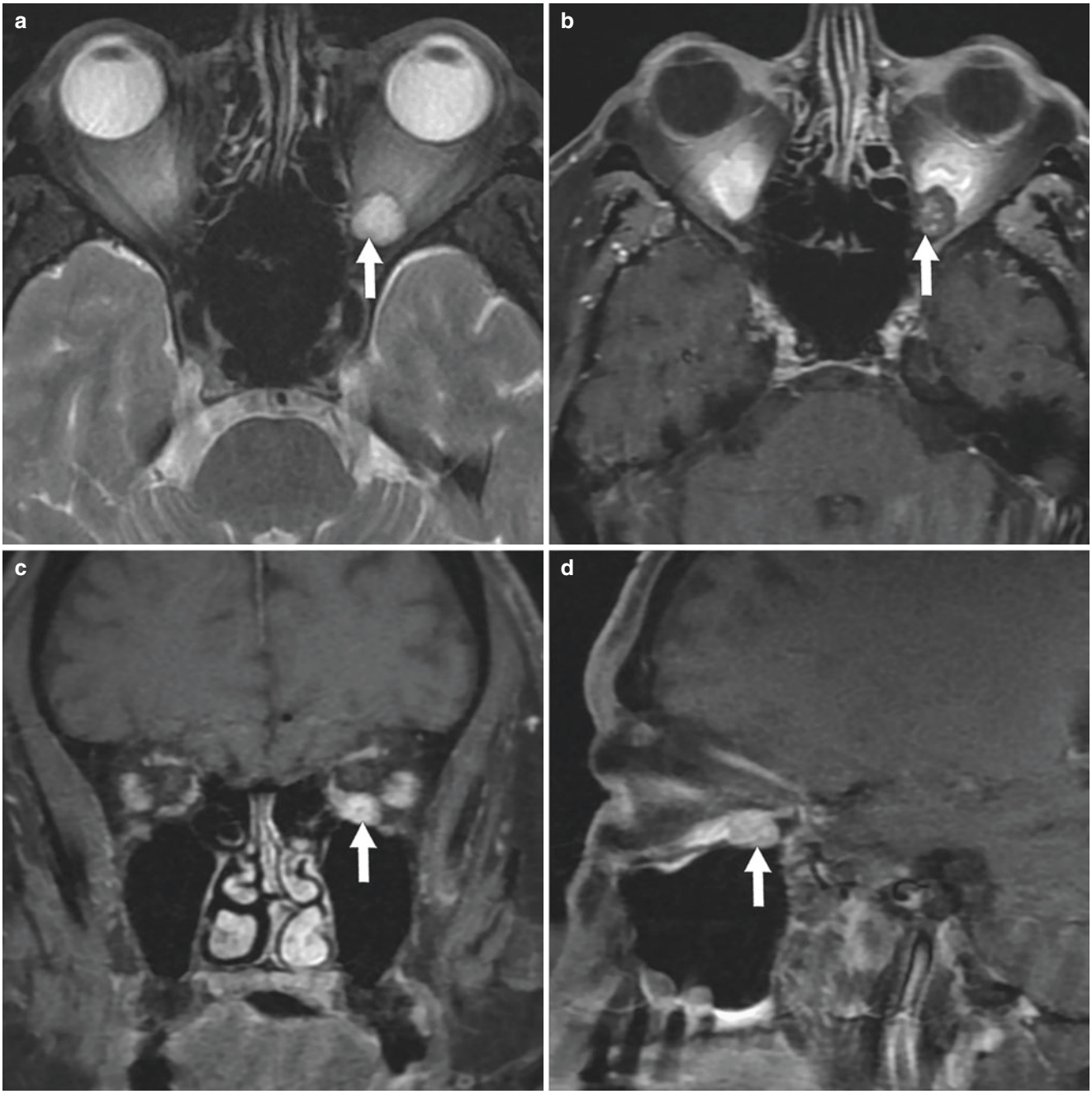

Fig. 4.34 A 72-year-old male with treated retroperitoneal liposarcoma who underwent MRI for vertigo, which showed an incidental left orbital venous malformation. (**a**) Axial T2 MRI with fat saturation shows a **hyperintense lesion in the left orbital apex** (arrows). (**b–d**) Axial, coronal, and sagittal T1 post-contrast MRI with fat saturation shows **gradual filling of the venous malformation with contrast on sequential series** (arrows)

Fig. 4.35 A 46-year-old male who underwent MRI for headaches which showed a left orbital venous malformation. (**a**) Axial T2 MRI with fat saturation shows a **hyperintense lesion in the intraconal space of the left orbit** (arrows). (**b**, **c**) Axial and sagittal T1 post-contrast MRI with fat saturation show **gradual filling of the venous malformation with contrast on sequential series** (arrows)

Key Points

- Important to **distinguish between venous, venolymphatic, and arteriovenous malformations, and varices**. Different management strategies are appropriate, depending on the type of vascular lesion.
- **Phleboliths can appear as signal voids** and lead to the misdiagnosis of this low-flow lesion as a high-flow lesion.
- **T2 hyperintense with delayed filling of contrast**.

Venolymphatic Malformation

Figure 4.36 shows a case of an orbital venolymphatic malformation.

Background

- A **venolymphatic malformation (VLM)** is a **slow-flow vascular malformation** arising from the pluripotent venous anlage that develops into both venous and lymphatic structures.
- Consists of **endothelial-lined lymph-filled vascular channels** with variable luminal diameters [147].

Presentation

- VLMs may be evident at birth but **usually manifest in infancy or childhood** [148].
- Females and males are affected with an equal frequency [149].
- A VLM within the orbit **may enlarge over time leading** to **progressive proptosis, eye movement restriction, or globe displacement.**
- **May present abruptly from hemorrhage** that may occur following minor trauma, or infection or develop spontaneously, leading to acute proptosis and occasionally optic nerve compression [150].

Imaging

- **Fluid-fluid levels within multiple cysts arising from hemorrhage of various ages is almost pathognomonic of a VLM**.
- Orbital VLMs are isolated from the normal orbital vasculature and **unaffected by postural changes**, differentiating them from varices [149].
- **Unencapsulated and therefore can be multicompartmental**, often involving both the intraconal and extraconal spaces [149].

CT

- VLMs are multicompartmental, not well-circumscribed. **Lymphatic components demonstrate minimal enhancement. Venous component enhances**.
- **Phleboliths** can be present [151].

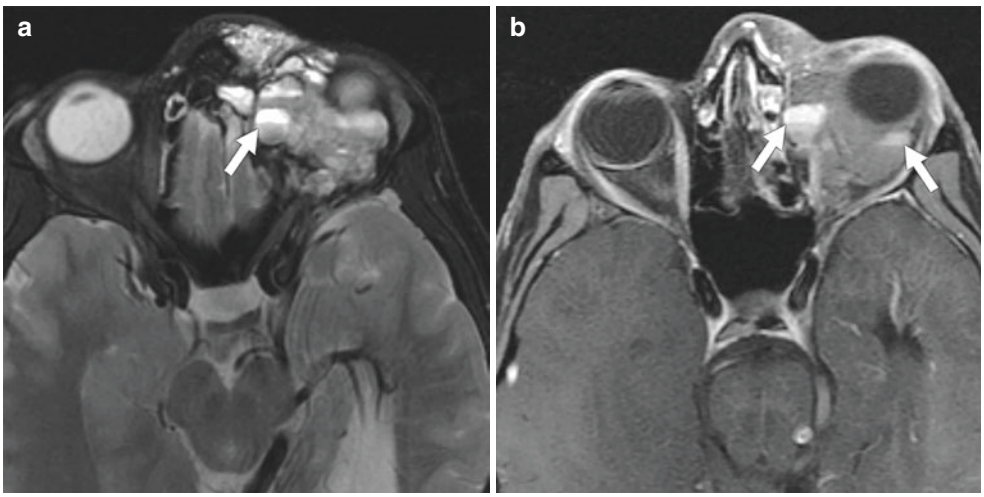

Fig. 4.36 A 19-year-old male with increasing proptosis related to a left orbital venolymphatic malformation. (**a**) Axial T2 MRI with fat saturation shows a lobulated mass in the superior left orbit with **multiple cysts containing fluid-fluid levels** (arrows). (**b**) Axial T1 post-contrast MRI with fat saturation shows **multicompartment involvement and cysts with fluid-fluid levels** (arrows)

MRI

- **Fluid-fluid levels within cysts** related to hemorrhages of various ages [149].
- T1 images demonstrate lymphatic and proteinaceous fluid.
- T2 fat-suppressed images best show non-hemorrhagic fluid [146].

Key Points

- **Phleboliths can appear as flow voids**, leading to the misdiagnosis of a high-flow lesion.
- Important to **distinguish between venous, venolymphatic, and arteriovenous malformations, and varices**. Different management strategies are appropriate depending on the type of vascular lesion.
- **VLMs can be treated with intralesional sclerotherapy**.
- **Comment on the need for additional studies** such as CT/MR angiography for **better characterization of the lesion**.

Varix

Figures 4.37 shows a case of an orbital varix.

Background

- Varices result from a **presumed congenital weakness of the post-capillary venous wall**, leading to the proliferation of venous components and marked dilation of the orbital veins [152].

Presentation

- **Presents in the second or third decade** with no gender bias [152].
- **Most varices communicate with the venous system** [150].

Imaging

- **Smooth contours** may appear club-like, triangular, segmentally dilated, or as a tangled vessel mass.
- **Maneuvers that increase venous pressure** (e.g., scanning with prone positioning or during the Valsalva maneuver) **demonstrate distension of varix** [150, 153].

CT

- **Involved veins have a normal appearance or mild enlargement**.

MRI

- **T1 hypo- to hyperintense and T2 hyperintense with intense enhancement** [150].

Key Points

- Important to **distinguish between venous, venolymphatic, and arteriovenous malformations, and varices**. Different management strategies are appropriate depending on type of vascular lesion.

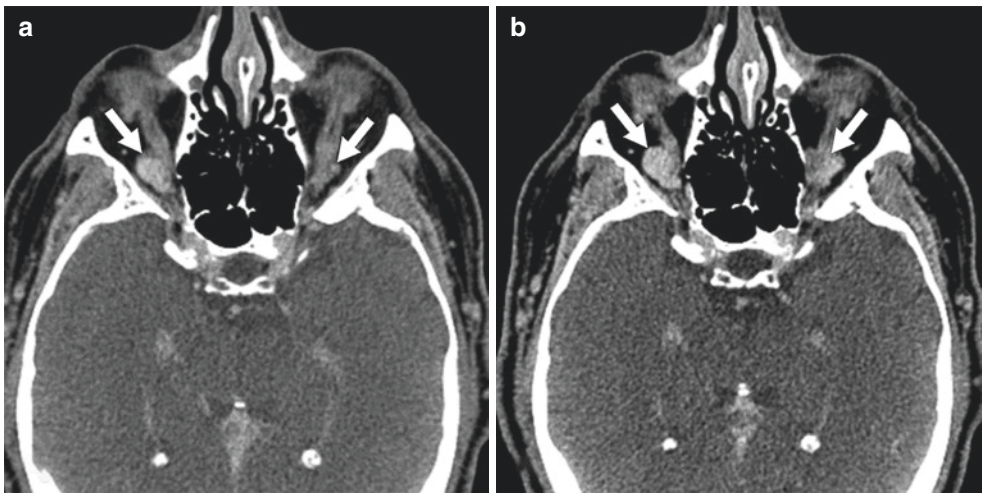

Fig. 4.37 A 61-year-old male with anaplastic thyroid carcinoma and incidentally discovered bilateral orbital varices. (**a**) Axial CT with contrast, soft tissue window shows **homogeneously enhancing lesions in the posterior orbits** (arrows). (**b**) Axial CT with contrast, soft tissue window while performing the **Valsalva maneuver shows enlargement of the varices** (arrows)

- **Valsalva maneuvers** may demonstrate distension of varix.

Arteriovenous Malformation

Figure 4.38 shows a case of an arteriovenous malformation involving the orbit.

Background

- Arteriovenous malformations (AVMs) feature a **nidus at the confluence of feeding arteries and draining veins without intervening capillaries** [154, 155].
- **Present at birth in a quiescent stage and do not present clinically until childhood or adulthood** [156].
- **Growth of the AVM** may be exacerbated by hormonal changes of puberty or pregnancy, or result from trauma, thrombosis, or infection [157].

Presentation

- AVMs are **high-flow vascular lesions**.
- **Symptoms** such as pain, bleeding, and overgrowth **depend on the degree of arteriovenous shunting** [155].
- Facial AVMs involving the skin or facial bones may **cause facial asymmetry, bleeding, or skin and mucosal ulcerations that can become secondarily infected** [158].

Imaging

- **Rapid filling of an AVM with contrast reaching the venous components during the arterial phase** [159].

CT

- **Feeding arteries and draining veins** can be visualized especially with CT angiography [158].

MRI

- **Serpiginous dilated vessels** with feeding arteries and draining veins.
- **Lack a well-defined mass** and appear as **flow voids, indicating the high-flow components** [156].
- **Associated T1 signal hyperintensity** may represent hemorrhage, intravascular thrombus, or flow-related enhancement [160].

Key Points

- **High-flow vascular lesion**.
- Important to **distinguish between venous, venolymphatic, and arteriovenous malformations, and varices**. Different management strategies are appropriate depending on type of vascular lesion.
- AVM **may benefit from pre-operative embolization**.

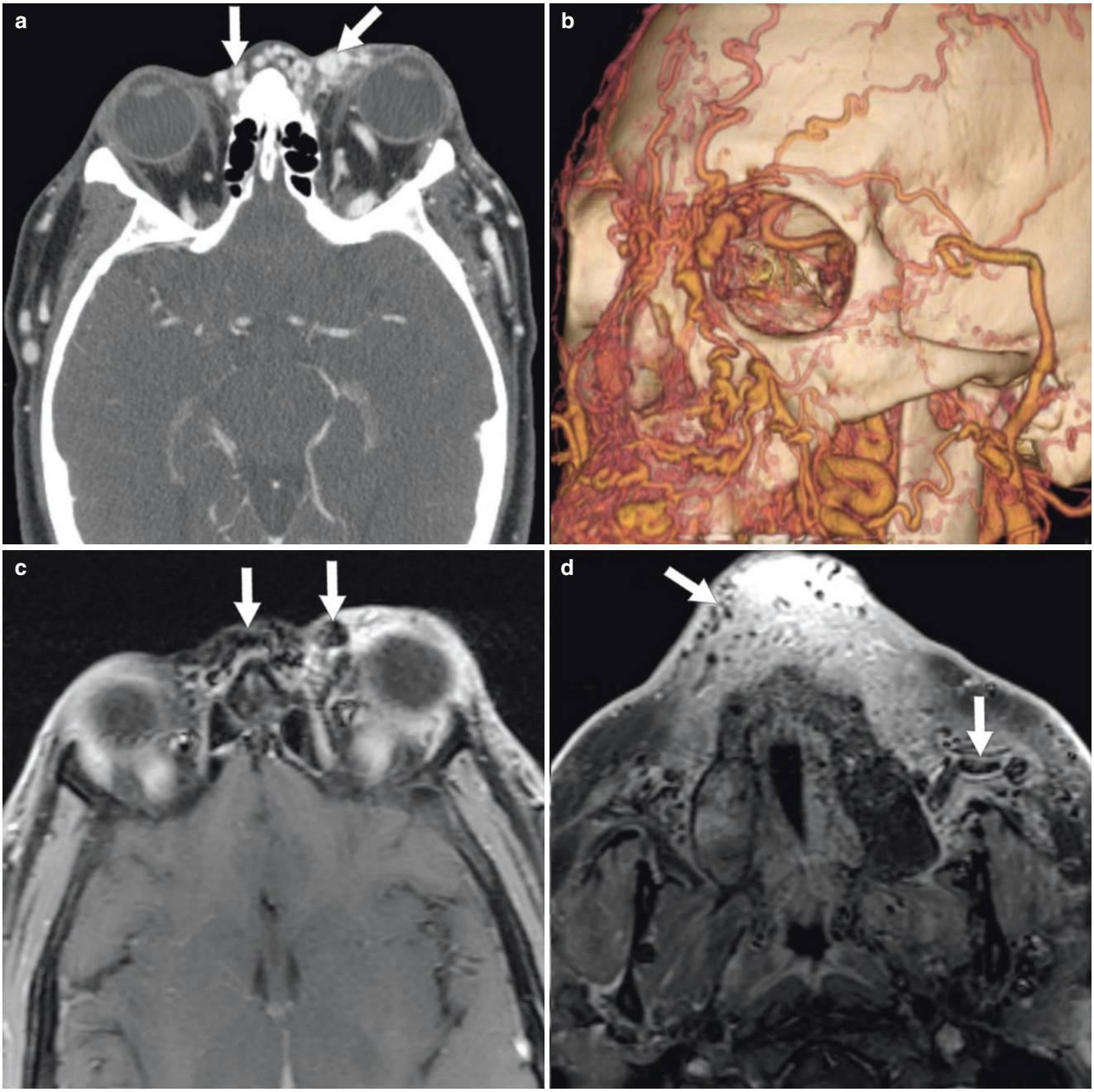

Fig. 4.38 A 28-year-old male with a congenital arteriovenous malformation and vision loss in the left eye. (**a**) Axial CT with contrast, soft tissue window shows **multiple dilated enhancing vessels about the face** (arrows). (**b**) Volume-rendered CT with contrast shows **serpiginous dilated vessels about the face and orbit**. (**c**, **d**) Axial T1 post-contrast MRI with fat saturation shows the **hypointense appearance of the vessels consistent with high flow vascular components** (arrows)

- **Comment on the need for additional studies such as CT/MR angiography for better characterization of the lesion**.

Superior Ophthalmic Vein Thrombosis

Figure 4.39 shows cases of superior ophthalmic vein thrombosis.

Background

- Superior ophthalmic vein thrombosis is extremely rare with **potentially devastating consequences** [161, 162].
- **Etiologies**: orbital cellulitis, paranasal sinusitis, trauma, cavernous sinus thrombosis, cavernous sinus thrombosis fistula, orbital neoplasm, hypercoagulable states, and Tolosa–Hunt syndrome [161].

Presentation

- **Symptoms**: periorbital edema, proptosis, globe dystopia, ophthalmoplegia, ptosis, proptosis, and chemosis (conjunctival edema) [161].

Imaging

- **Superior ophthalmic vein appears dilated and thrombotic**.
- There may be evidence of sinusitis or cellulitis or a history of functional sinus surgery.

CT/MRI

- **Linear filling defect in a dilated superior ophthalmic vein** related to the thrombosis on CT and MR venography.
- Superior ophthalmic vein and/or cavernous sinus thrombosis **may not be evident in the early stages**.
- Some authors believe that MRI is more sensitive for diagnosis [163].

Key Points

- **Search for imaging signs of the potential causes of superior ophthalmic vein thrombosis**, e.g., orbital cellulitis, sinusitis, cavernous sinus thrombosis/fistula, or an orbital lesion.

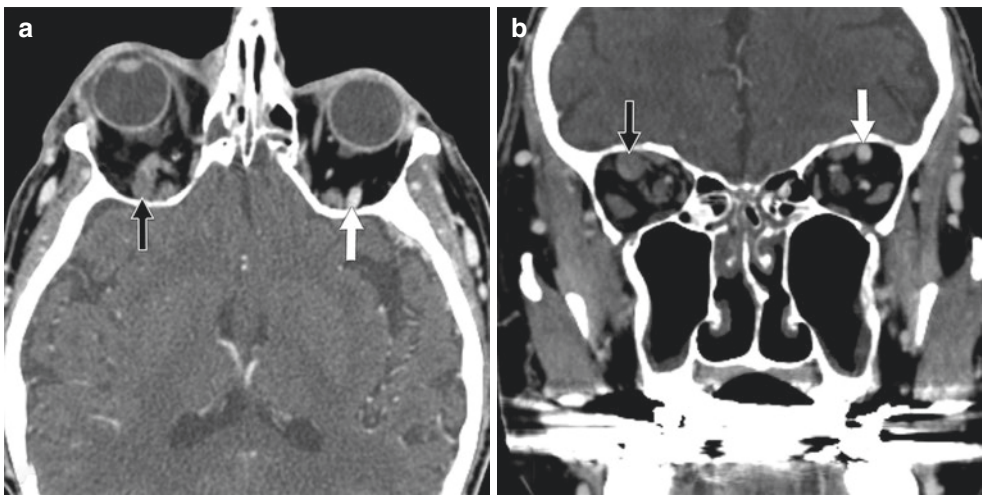

Fig. 4.39 A 71-year-old male with right orbital swelling, vision loss, and thrombocytosis (elevated platelet count). (**a**, **b**) Axial and coronal CT with contrast, soft tissue window shows **contrast filling the left superior ophthalmic vein** (white arrows) and **lack of enhancement in the dilated right superior ophthalmic vein** (black arrows). Note **proptosis** of the right globe and enlargement of the right extra-ocular muscles

References

1. Ferry JA, Fung CY, Zukerberg L, Lucarelli MJ, Hasserjian RP, Preffer FI, et al. Lymphoma of the ocular adnexa: a study of 353 cases. Am J Surg Pathol. 2007;31:170–84. https://doi.org/10.1097/01.pas.0000213350.49767.46.
2. Sjö LD. Ophthalmic lymphoma: epidemiology and pathogenesis. Acta Ophthalmol. 2009;87:1–20. https://doi.org/10.1111/j.1755-3768.2008.01478.x.
3. Olsen TG, Holm F, Mikkelsen LH, Rasmussen PK, Coupland SE, Esmaeli B, et al. Orbital lymphoma-an international multicenter retrospective study. Am J Ophthalmol. 2019;199:44–57. https://doi.org/10.1016/j.ajo.2018.11.002.
4. Purohit BS, Vargas MI, Ailianou A, Merlini L, Poletti PA, Platon A, et al. Orbital tumours and tumour-like lesions: exploring the armamentarium of multiparametric imaging. Insights Imaging. 2016;7:43–68. https://doi.org/10.1007/s13244-015-0443-8.
5. Tailor TD, Gupta D, Dalley RW, Keene CD, Anzai Y. Orbital neoplasms in adults: clinical, radiologic, and pathologic review. Radiographics. 2013;33:1739–58. https://doi.org/10.1148/rg.336135502.
6. Haradome K, Haradome H, Usui Y, Ueda S, Kwee TC, Saito K, et al. Orbital lymphoproliferative disorders (OLPDs): value of MR imaging for differentiating orbital lymphoma from benign OPLDs. AJNR Am J Neuroradiol. 2014;35:1976–82. https://doi.org/10.3174/ajnr.A3986.
7. Hoffmann M, Kletter K, Diemling M, Becherer A, Pfeffel F, Petkov V, et al. Positron emission tomography with fluorine-18-2-fluoro-2-deoxy-D-glucose (F18-FDG) does not visualize extranodal B-cell lymphoma of the mucosa-associated lymphoid tissue (MALT)-type. Ann Oncol. 1999;10:1185–9. https://doi.org/10.1023/a:1008312726163.
8. Almuhaideb A, Papathanasiou N, Bomanji J. 18F-FDG PET/CT imaging in oncology. Ann Saudi Med. 2011;31:3–13. https://doi.org/10.4103/0256-4947.75771.
9. Koshy J, John MJ, Thomas S, Kaur G, Batra N, Xavier WJ. Ophthalmic manifestations of acute and chronic leukemias presenting to a tertiary care center in India. Indian J Ophthalmol. 2015;63:659–64. https://doi.org/10.4103/0301-4738.169789.
10. Bidar M, Wilson MW, Laquis SJ, Wilson TD, Fleming JC, Wesley RE, et al. Clinical and imaging characteristics of orbital leukemic tumors. Ophthalmic Plast Reconstr Surg. 2007;23:87–93. https://doi.org/10.1097/IOP.0b013e3180333a85.
11. Reddy SC, Jackson N, Menon BS. Ocular involvement in leukemia—a study of 288 cases. Ophthalmologica. 2003;217:441–5. https://doi.org/10.1159/000073077.
12. Schachat AP, Markowitz JA, Guyer DR, Burke PJ, Karp JE, Graham ML. Ophthalmic manifestations of leukemia. Arch Ophthalmol. 1989;107:697–700. https://doi.org/10.1001/archopht.1989.01070010715033.
13. Chung EM, Murphey MD, Specht CS, Cube R, Smirniotopoulos JG. From the Archives of the AFIP. Pediatric orbit tumors and tumorlike lesions: osseous lesions of the orbit. Radiographics. 2008;28:1193–214. https://doi.org/10.1148/rg.284085013.
14. Ohanian M, Borthakur G, Quintas-Cardama A, Mathisen M, Cortés JE, Estrov Z, et al. Ocular granulocytic sarcoma: a case report and literature review of ocular extramedullary acute myeloid leukemia. Clin Lymphoma Myeloma Leuk. 2013;13:93–6. https://doi.org/10.1016/j.clml.2012.07.008.
15. Charif Chefchaouni M, Belmekki M, Hajji Z, Tahiri H, Amrani R, El Bakkali M, et al. Manifestations ophtalmologiques des leucémies aiguës [Ophthalmic manifestations of acute leukemia]. J Fr Ophtalmol. 2002;25:62–6.
16. Singh AD. The prevalence of ocular disease in chronic lymphocytic leukaemia. Eye (Lond). 2003;17:3–4. https://doi.org/10.1038/sj.eye.6700278.
17. Pui MH, Fletcher BD, Langston JW. Granulocytic sarcoma in childhood leukemia: imaging features. Radiology. 1994;190:698–702.
18. Natarajan A, Chandra P, Purandare N, Agrawal A, Shah S, Puranik A, et al. Role of fluorodeoxyglucose positron emission tomography/computed tomography in various orbital malignancies. Indian J Nucl Med. 2018;33(2):118–24. https://doi.org/10.4103/ijnm.IJNM_135_17.
19. Jha P, Frölich AM, McCarville B, Navarro OM, Babyn P, Goldsby R, et al. Unusual association of alveolar rhabdomyosarcoma with pancreatic metastasis: emerging role of PET-CT in tumor staging. Pediatr Radiol. 2010;40:1380–6. https://doi.org/10.1007/s00247-010-1572-3.
20. Freling NJ, Merks JH, Saeed P, Balm AJ, Bras J, Pieters BR, et al. Imaging findings in craniofacial childhood rhabdomyosarcoma. Pediatr Radiol. 2010;40:1723–38; quiz 1855. https://doi.org/10.1007/s00247-010-1787-3.
21. Mennel S, Meyer CH, Peter S, Schmidt JC, Kroll P. Current treatment modalities for exudative retinal hamartomas secondary to tuberous sclerosis: review of the literature. Acta Ophthalmol Scand. 2007;85(2):127–32. https://doi.org/10.1111/j.1600-0420.2006.00781.x.
22. Huh WW, Mahajan A. Ophthalmic oncology. In: Esmaeli B, editor. Ophthalmic oncology. Boston, MA: Springer; 2011. p. 61–7.
23. Allen SD, Moskovic EC, Fisher C, Thomas JM. Adult rhabdomyosarcoma: cross-sectional imaging findings including histopathologic correlation. AJR Am J Roentgenol. 2007;189:371–7. https://doi.org/10.2214/AJR.07.2065.
24. Hagiwara A, Inoue Y, Nakayama T, Yamato K, Nemoto Y, Shakudo M, et al. The "botryoid sign": a characteristic feature of rhabdomyosarcomas in the head and neck. Neuroradiology. 2001;43:331–5. https://doi.org/10.1007/s002340000464.
25. La Quaglia MP, Heller G, Ghavimi F, Casper ES, Vlamis V, Hajdu S, et al. The effect of age at diagnosis on outcome in rhabdomyosarcoma. Cancer. 1994;73:109–17. https://doi.org/10.1002/1097-0142(19940101)73:1<109::aid-cncr2820730120>3.0.co;2-s.
26. Rao AA, Naheedy JH, Chen JY, Robbins SL, Ramkumar HL. A clinical update and radiologic review of pediatric orbital and ocular tumors. J Oncol. 2013;2013:975908. https://doi.org/10.1155/2013/975908.
27. Wippold FJ 2nd, Lubner M, Perrin RJ, Lämmle M, Perry A. Neuropathology for the neuroradiologist: Antoni A and Antoni B tissue patterns. AJNR Am J Neuroradiol. 2007;28:1633–8. https://doi.org/10.3174/ajnr.A0682.
28. Wilson MP, Katlariwala P, Low G, Murad MH, McInnes MDF, Jacques L, et al. Diagnostic accuracy of MRI for the detection of malignant peripheral nerve sheath tumors: a systematic review and meta-analysis. AJR Am J Roentgenol. 2021;217:31–9. https://doi.org/10.2214/AJR.20.23403.
29. Skolnik AD, Loevner LA, Sampathu DM, Newman JG, Lee JY, Bagley LJ, et al. Cranial nerve schwannomas: diagnostic imaging approach. Radiographics. 2016;36:1463–77. https://doi.org/10.1148/rg.2016150199.
30. Baehring JM, Betensky RA, Batchelor TT. Malignant peripheral nerve sheath tumor: the clinical spectrum and outcome of treatment. Neurology. 2003;61:696–8. https://doi.org/10.1212/01.wnl.0000078813.05925.2c.
31. Kapur R, Mafee MF, Lamba R, Edward DP. Orbital schwannoma and neurofibroma: role of imaging. Neuroimaging Clin N Am. 2005;15:159–74. https://doi.org/10.1016/j.nic.2005.02.004.
32. Chung SY, Kim DI, Lee BH, Yoon PH, Jeon P, Chung TS. Facial nerve schwannomas: CT and MR findings. Yonsei Med J. 1998;39:148–53. https://doi.org/10.3349/ymj.1998.39.2.148.
33. Koga H, Matsumoto S, Manabe J, Tanizawa T, Kawaguchi N. Definition of the target sign and its use for the diagnosis of

schwannomas. Clin Orthop Relat Res. 2007;464:224–9. https://doi.org/10.1097/BLO.0b013e3181583422.
34. Dewey BJ, Howe BM, Spinner RJ, Johnson GB, Nathan MA, Wenger DE, et al. FDG PET/CT and MRI features of pathologically proven schwannomas. Clin Nucl Med. 2021;46:289–96. https://doi.org/10.1097/RLU.0000000000003485.
35. Alkatan HM, Alsalamah AK, Almizel A, Alshomar KM, Maktabi AM, ElKhamary SM, et al. Orbital solitary fibrous tumors: a multi-centered histopathological and immunohistochemical analysis with radiological description. Ann Saudi Med. 2020;40:227–33. https://doi.org/10.5144/0256-4947.2020.227.
36. Lahon B, Mercier O, Fadel E, Ghigna MR, Petkova B, Mussot S, et al. Solitary fibrous tumor of the pleura: outcomes of 157 complete resections in a single center. Ann Thorac Surg. 2012;94:394–400. https://doi.org/10.1016/j.athoracsur.2012.04.028.
37. Gold JS, Antonescu CR, Hajdu C, Ferrone CR, Hussain M, Lewis JJ, et al. Clinicopathologic correlates of solitary fibrous tumors. Cancer. 2002;94:1057–68.
38. Demicco EG, Park MS, Araujo DM, Fox PS, Bassett RL, Pollock RE, et al. Solitary fibrous tumor: a clinicopathological study of 110 cases and proposed risk assessment model. Mod Pathol. 2012;25:1298–306. https://doi.org/10.1038/modpathol.2012.83.
39. Polito E, Tosi GM, Toti P, Schürfeld K, Caporossi A. Orbital solitary fibrous tumor with aggressive behavior Three cases and review of the literature. Graefes Arch Clin Exp Ophthalmol. 2002;240:570–4. https://doi.org/10.1007/s00417-002-0486-7.
40. Krishnakumar S, Subramanian N, Mohan ER, Mahesh L, Biswas J, Rao NA. Solitary fibrous tumor of the orbit: a clinicopathologic study of six cases with review of the literature. Surv Ophthalmol. 2003;48:544–54. https://doi.org/10.1016/s0039-6257(03)00087-0.
41. Yang BT, Wang YZ, Dong JY, Wang XY, Wang ZC. MRI study of solitary fibrous tumor in the orbit. AJR Am J Roentgenol. 2012;199:W506–11. https://doi.org/10.2214/AJR.11.8477.
42. Kim HJ, Kim HJ, Kim YD, Yim YJ, Kim ST, Jeon P, et al. Solitary fibrous tumor of the orbit: CT and MR imaging findings. AJNR Am J Neuroradiol. 2008;29:857–62. https://doi.org/10.3174/ajnr.A0961.
43. Liu Y, Li K, Shi H, Tao X. Solitary fibrous tumours in the extracranial head and neck region: correlation of CT and MR features with pathologic findings. Radiol Med. 2014;119:910–9. https://doi.org/10.1007/s11547-014-0409-9.
44. Khandelwal A, Virmani V, Amin MS, George U, Khandelwal K, Gorsi U. Radiology-pathology conference: malignant solitary fibrous tumor of the seminal vesicle. Clin Imaging. 2013;37:409–13. https://doi.org/10.1016/j.clinimag.2012.04.027.
45. Liu Y, Tao X, Shi H, Li K. MRI findings of solitary fibrous tumours in the head and neck region. Dentomaxillofac Radiol. 2014;43:20130415. https://doi.org/10.1259/dmfr.20130415.
46. El Ouni F, Jemni H, Trabelsi A, Ben Maitig M, Arifa N, Ben Rhouma K, et al. Liposarcoma of the extremities: MR imaging features and their correlation with pathologic data. Orthop Traumatol Surg Res. 2010;96:876–83. https://doi.org/10.1016/j.otsr.2010.05.010.
47. Drevelegas A, Pilavaki M, Chourmouzi D. Lipomatous tumors of soft tissue: MR appearance with histological correlation. Eur J Radiol. 2004;50:257–67. https://doi.org/10.1016/j.ejrad.2004.01.022.
48. Walker EA, Salesky JS, Fenton ME, Murphey MD. Magnetic resonance imaging of malignant soft tissue neoplasms in the adult. Radiol Clin N Am. 2011;49:1219–34, vi. https://doi.org/10.1016/j.rcl.2011.07.006.
49. Davis EC, Ballo MT, Luna MA, Patel SR, Roberts DB, Nong X, et al. Liposarcoma of the head and neck: The University of Texas M. D. Anderson Cancer Center experience. Head Neck. 2009;31:28–36. https://doi.org/10.1002/hed.20923.
50. Murphey MD, Arcara LK, Fanburg-Smith J. From the archives of the AFIP: imaging of musculoskeletal liposarcoma with radiologic-pathologic correlation. Radiographics. 2005;25:1371–95. https://doi.org/10.1148/rg.255055106.
51. Uhl M, Roeren T, Schneider B, Kauffmann GW. Magnetresonanztomographie der Liposarkome [Magnetic resonance tomography of liposarcoma]. Rofo. 1996;165(2):144–7. https://doi.org/10.1055/s-2007-1015729.
52. Kennedy RE. An evaluation of 820 orbital cases. Trans Am Ophthalmol Soc. 1984;82:134–57.
53. Char DH, Miller T, Kroll S. Orbital metastases: diagnosis and course. Br J Ophthalmol. 1997;81:386–90. https://doi.org/10.1136/bjo.81.5.386.
54. Günalp I, Gündüz K. Metastatic orbital tumors. Jpn J Ophthalmol. 1995;39:65–70.
55. Shields CL, Shields JA, Peggs M. Tumors metastatic to the orbit. Ophthalmic Plast Reconstr Surg. 1988;4:73–80. https://doi.org/10.1097/00002341-198804020-00003.
56. Bowns GT, Walls RP, Murphree AL, Ortega J. Neonatal neuroblastoma metastatic to the iris. Cancer. 1983;52(5):929–31. https://doi.org/10.1002/1097-0142(19830901)52:5<929::aid-cncr2820520531>3.0.co;2-h.
57. Ng E, Ilsen PF. Orbital metastases. Optometry. 2010;81:647–57. https://doi.org/10.1016/j.optm.2010.07.026.
58. Ahmad SM, Esmaeli B. Metastatic tumors of the orbit and ocular adnexa. Curr Opin Ophthalmol. 2007;18:405–13. https://doi.org/10.1097/ICU.0b013e3282c5077c.
59. Zografos L, Ducrey N, Beati D, Schalenbourg A, Spahn B, Balmer A, et al. Metastatic melanoma in the eye and orbit. Ophthalmology. 2003;110:2245–56. https://doi.org/10.1016/j.ophtha.2003.05.004.
60. Crisostomo S, Cardigos J, Fernandes DH, Luís ME, Pires GN, Duarte AF, et al. Bilateral metastases to the extraocular muscles from small cell lung carcinoma. Arq Bras Oftalmol. 2019;82:422–4. https://doi.org/10.5935/0004-2749.20190081.
61. Koeller KK, Smirniotopoulos JG. Orbital masses. Semin Ultrasound CT MR. 1998;19:272–91. https://doi.org/10.1016/s0887-2171(98)90012-9.
62. Muzaffar R, Shousha MA, Sarajlic L, Osman MM. Ophthalmologic abnormalities on FDG-PET/CT: a pictorial essay. Cancer Imaging. 2013;13:100–12. https://doi.org/10.1102/1470-7330.2013.0010.
63. Smith TJ, Hegedüs L. Graves' Disease. N Engl J Med. 2016;375:1552–65. https://doi.org/10.1056/NEJMra1510030.
64. Ferrari SM, Ruffilli I, Elia G, Ragusa F, Paparo SR, Patrizio A, et al. Chemokines in hyperthyroidism. J Clin Transl Endocrinol. 2019;16:100196. https://doi.org/10.1016/j.jcte.2019.100196.
65. Lindgren AL, Sidhu S, Welsh KM. Periorbital myxedema treated with intralesional hyaluronidase. Am J Ophthalmol Case Rep. 2020;19:100751. https://doi.org/10.1016/j.ajoc.2020.100751.
66. Wei Y, Kang XL, Del Monte MA. Enlargement of the superior rectus and superior oblique muscles causes intorsion in Graves' eye disease. Br J Ophthalmol. 2016;100(9):1280–4. https://doi.org/10.1136/bjophthalmol-2015-307704.
67. Antonelli A, Ferrari SM, Ragusa F, Elia G, Paparo SR, Ruffilli I, et al. Graves' disease: epidemiology, genetic and environmental risk factors and viruses. Best Pract Res Clin Endocrinol Metab. 2020;34:101387. https://doi.org/10.1016/j.beem.2020.101387.
68. Devereaux D, Tewelde SZ. Hyperthyroidism and thyrotoxicosis. Emerg Med Clin North Am. 2014;32:277–92. https://doi.org/10.1016/j.emc.2013.12.001.
69. Boelaert K, Torlinska B, Holder RL, Franklyn JA. Older subjects with hyperthyroidism present with a paucity of symptoms and signs: a large cross-sectional study. J Clin Endocrinol Metab. 2010;95:2715–26. https://doi.org/10.1210/jc.2009-2495.

70. Frueh BR, Musch DC, Garber FW. Lid retraction and levator aponeurosis defects in Graves' eye disease. Ophthalmic Surg. 1986;17:216–20.
71. Bartley GB. The epidemiologic characteristics and clinical course of ophthalmopathy associated with autoimmune thyroid disease in Olmsted County, Minnesota. Trans Am Ophthalmol Soc. 1994;92:477–588.
72. Rootman J. Diseases of the orbit: a multidisciplinary approach. Philadelphia: Lippincott; 1988. p. 143–240.
73. Feldon SE, Lee CP, Muramatsu SK, Weiner JM. Quantitative computed tomography of Graves' ophthalmopathy. Extraocular muscle and orbital fat in development of optic neuropathy. Arch Ophthalmol. 1985;103:213–5. https://doi.org/10.1001/archopht.1985.01050020065021.
74. Barrett L, Glatt HJ, Burde RM, Gado MH. Optic nerve dysfunction in thyroid eye disease: CT. Radiology. 1988;167:503–7. https://doi.org/10.1148/radiology.167.2.3357962.
75. Nugent RA, Belkin RI, Neigel JM, Rootman J, Robertson WD, Spinelli J, et al. Graves orbitopathy: correlation of CT and clinical findings. Radiology. 1990;177:675–82. https://doi.org/10.1148/radiology.177.3.2243967.
76. Birchall D, Goodall KL, Noble JL, Jackson A. Graves ophthalmopathy: intracranial fat prolapse on CT images as an indicator of optic nerve compression. Radiology. 1996;200:123–7. https://doi.org/10.1148/radiology.200.1.8657899.
77. Gonçalves AC, Silva LN, Gebrim EM, Monteiro ML. Quantification of orbital apex crowding for screening of dysthyroid optic neuropathy using multidetector CT. AJNR Am J Neuroradiol. 2012;33:1602–7. https://doi.org/10.3174/ajnr.A3029.
78. Dodds NI, Atcha AW, Birchall D, Jackson A. Use of high-resolution MRI of the optic nerve in Graves' ophthalmopathy. Br J Radiol. 2009;82:541–4. https://doi.org/10.1259/bjr/56958444.
79. Tan NYQ, Leong YY, Lang SS, Htoon ZM, Young SM, Sundar G. Radiologic parameters of orbital bone remodeling in thyroid eye disease. Invest Ophthalmol Vis Sci. 2017;58:2527–33. https://doi.org/10.1167/iovs.16-21035.
80. Kvetny J, Puhakka KB, Røhl L. Magnetic resonance imaging determination of extraocular eye muscle volume in patients with thyroid-associated ophthalmopathy and proptosis. Acta Ophthalmol Scand. 2006;84:419–23. https://doi.org/10.1111/j.1600-0420.2005.00617.x.
81. Tortora F, Cirillo M, Ferrara M, Belfiore MP, Carella C, Caranci F, et al. Disease activity in Graves' ophthalmopathy: diagnosis with orbital MR imaging and correlation with clinical score. Neuroradiol J. 2013;26:555–64. https://doi.org/10.1177/197140091302600.
82. Rothfus WE, Curtin HD. Extraocular muscle enlargement: a CT review. Radiology. 1984;151:677–81. https://doi.org/10.1148/radiology.151.3.6546996.
83. Yuen SJ, Rubin PA. Idiopathic orbital inflammation: distribution, clinical features, and treatment outcome. Arch Ophthalmol. 2003;121:491–9. https://doi.org/10.1001/archopht.121.4.491.
84. Weber AL, Romo LV, Sabates NR. Pseudotumor of the orbit. Clinical, pathologic, and radiologic evaluation. Radiol Clin N Am. 1999;37:151–68, xi. https://doi.org/10.1016/s0033-8389(05)70084-1.
85. Ferreira TA, Saraiva P, Genders SW, Buchem MV, Luyten GPM, Beenakker JW. CT and MR imaging of orbital inflammation. Neuroradiology. 2018;60:1253–66. https://doi.org/10.1007/s00234-018-2103-4.
86. Li Y, Lip G, Chong V, Yuan J, Ding Z. Idiopathic orbital inflammation syndrome with retro-orbital involvement: a retrospective study of eight patients. PLoS One. 2013;8:e57126. https://doi.org/10.1371/journal.pone.0057126.
87. Narla LD, Newman B, Spottswood SS, Narla S, Kolli R. Inflammatory pseudotumor. Radiographics. 2003;23:719–29. https://doi.org/10.1148/rg.233025073.
88. Sepahdari AR, Aakalu VK, Setabutr P, Shiehmorteza M, Naheedy JH, Mafee MF. Indeterminate orbital masses: restricted diffusion at MR imaging with echo-planar diffusion-weighted imaging predicts malignancy. Radiology. 2010;256:554–64. https://doi.org/10.1148/radiol.10091956.
89. Umehara H, Okazaki K, Masaki Y, Kawano M, Yamamoto M, Saeki T, et al. Comprehensive diagnostic criteria for IgG4-related disease (IgG4-RD), 2011. Mod Rheumatol. 2012;22:21–30. https://doi.org/10.1007/s10165-011-0571-z.
90. Stone JH, Zen Y, Deshpande V. IgG4-related disease. N Engl J Med. 2012;366:539–51. https://doi.org/10.1056/NEJMra1104650.
91. Tirelli G, Gardenal N, Gatto A, Quatela E, Del Piero GC. Head and neck immunoglobulin G4 related disease: systematic review. J Laryngol Otol. 2018;132:1046–50. https://doi.org/10.1017/S0022215118002153.
92. Fujita A, Sakai O, Chapman MN, Sugimoto H. IgG4-related disease of the head and neck: CT and MR imaging manifestations. Radiographics. 2012;32:1945–58. https://doi.org/10.1148/rg.327125032.
93. Hayashi Y, Moriyama M, Maehara T, Goto Y, Kawano S, Ohta M, et al. A case of mantle cell lymphoma presenting as IgG4-related dacryoadenitis and sialoadenitis, so-called Mikulicz's disease. World J Surg Oncol. 2015;13:225. https://doi.org/10.1186/s12957-015-0644-0.
94. Himi T, Takano K, Yamamoto M, Naishiro Y, Takahashi H. A novel concept of Mikulicz's disease as IgG4-related disease. Auris Nasus Larynx. 2012;39:9–17. https://doi.org/10.1016/j.anl.2011.01.023.
95. Ginat DT, Freitag SK, Kieff D, Grove A, Fay A, Cunnane M, Moonis G. Radiographic patterns of orbital involvement in IgG4-related disease. Ophthalmic Plast Reconstr Surg. 2013;29:261–6. https://doi.org/10.1097/IOP.0b013e31829165ad.
96. Tiegs-Heiden CA, Eckel LJ, Hunt CH, Diehn FE, Schwartz KM, Kallmes DF, et al. Immunoglobulin G4-related disease of the orbit: imaging features in 27 patients. AJNR Am J Neuroradiol. 2014;35(7):1393–7.
97. Zhao Z, Wang Y, Guan Z, Jin J, Huang F, Zhu J. Utility of FDG-PET/CT in the diagnosis of IgG4-related diseases. Clin Exp Rheumatol. 2016;34:119–25.
98. Rao DA, Dellaripa PF. Extrapulmonary manifestations of sarcoidosis. Rheum Dis Clin N Am. 2013;39:277–97. https://doi.org/10.1016/j.rdc.2013.02.007.
99. Obenauf CD, Shaw HE, Sydnor CF, Klintworth GK. Sarcoidosis and its ophthalmic manifestations. Am J Ophthalmol. 1978;86:648–55. https://doi.org/10.1016/0002-9394(78)90184-8.
100. Ganeshan D, Menias CO, Lubner MG, Pickhardt PJ, Sandrasegaran K, Bhalla S. Sarcoidosis from head to toe: what the radiologist needs to know. Radiographics. 2018;38:1180–200. https://doi.org/10.1148/rg.2018170157.
101. Bodaghi B, Touitou V, Fardeau C, Chapelon C, LeHoang P. Ocular sarcoidosis. Presse Med. 2012;41:e349–54. https://doi.org/10.1016/j.lpm.2012.04.004.
102. Evans M, Sharma O, LaBree L, Smith RE, Rao NA. Differences in clinical findings between Caucasians and African Americans with biopsy-proven sarcoidosis. Ophthalmology. 2007;114:325–33. https://doi.org/10.1016/j.ophtha.2006.05.074.
103. Collison JM, Miller NR, Green WR. Involvement of orbital tissues by sarcoid. Am J Ophthalmol. 1986;102:302–7. https://doi.org/10.1016/0002-9394(86)90002-4.
104. Patel S. Ocular sarcoidosis. Int Ophthalmol Clin. 2015;55:15–24. https://doi.org/10.1097/IIO.0000000000000069.

105. Mavrikakis I, Rootman J. Diverse clinical presentations of orbital sarcoid. Am J Ophthalmol. 2007;144:769–75. https://doi.org/10.1016/j.ajo.2007.07.019.
106. Pasadhika S, Rosenbaum JT. Ocular sarcoidosis. Clin Chest Med. 2015;36:669–83. https://doi.org/10.1016/j.ccm.2015.08.009.
107. Vettiyil B, Gupta N, Kumar R. Positron emission tomography imaging in sarcoidosis. World J Nucl Med. 2013;12:82–6. https://doi.org/10.4103/1450-1147.136731.
108. Chapman MN, Fujita A, Sung EK, Siegel C, Nadgir RN, Saito N, et al. Sarcoidosis in the head and neck: an illustrative review of clinical presentations and imaging findings. AJR Am J Roentgenol. 2017;208:66–75. https://doi.org/10.2214/AJR.16.16058.
109. Yang B, Yin Z, Chen S, Yuan F, Zhao W, Yang Y. Imaging diagnosis of orbital Wegener granulomatosis: a rare case report. Medicine (Baltimore). 2017;96:e6904. https://doi.org/10.1097/MD.0000000000006904.
110. Pakalniskis MG, Berg AD, Policeni BA, Gentry LR, Sato Y, Moritani T, et al. The many faces of granulomatosis with polyangiitis: a review of the head and neck imaging manifestations. AJR Am J Roentgenol. 2015;205:W619–29. https://doi.org/10.2214/AJR.14.13864.
111. Tarabishy AB, Schulte M, Papaliodis GN, Hoffman GS. Wegener's granulomatosis: clinical manifestations, differential diagnosis, and management of ocular and systemic disease. Surv Ophthalmol. 2010;55:429–44. https://doi.org/10.1016/j.survophthal.2009.12.003.
112. Colby TV, Tazelaar HD, Specks U, DeRemee RA. Nasal biopsy in Wegener's granulomatosis. Hum Pathol. 1991;22:101–4. https://doi.org/10.1016/0046-8177(91)90028-n.
113. Lovelace K, Cannon TC, Flynn S, Davis P, Schmucker T, Westfall CT. Optic neuropathy in patient with Wegener's granulomatosis. J Ark Med Soc. 2004;100:428–9.
114. Montecucco C, Caporali R, Pacchetti C, Turla M. Is Tolosa-Hunt syndrome a limited form of Wegener's granulomatosis? Report of two cases with anti-neutrophil cytoplasmic antibodies. Br J Rheumatol. 1993;32:640–1. https://doi.org/10.1093/rheumatology/32.7.640.
115. Schmidt J, Pulido JS, Matteson EL. Ocular manifestations of systemic disease: antineutrophil cytoplasmic antibody-associated vasculitis. Curr Opin Ophthalmol. 2011;22:489–95. https://doi.org/10.1097/ICU.0b013e32834bdfe2.
116. Holle JU, Gross WL. Neurological involvement in Wegener's granulomatosis. Curr Opin Rheumatol. 2011;23:7–11. https://doi.org/10.1097/BOR.0b013e32834115f9.
117. Grindler D, Cannady S, Batra PS. Computed tomography findings in sinonasal Wegener's granulomatosis. Am J Rhinol Allergy. 2009;23(5):497–501. https://doi.org/10.2500/ajra.2009.23.3359.
118. Owen RG, Treon SP, Al-Katib A, Fonseca R, Greipp PR, McMaster ML, et al. Clinicopathological definition of Waldenstrom's macroglobulinemia: consensus panel recommendations from the Second International Workshop on Waldenstrom's Macroglobulinemia. Semin Oncol. 2003;30:110–5. https://doi.org/10.1053/sonc.2003.50082.
119. Swerdlow SH, Campo E, Pileri SA, Harris NL, Stein H, Siebert R, et al. The 2016 revision of the World Health Organization classification of lymphoid neoplasms. Blood. 2016;127:2375–90. https://doi.org/10.1182/blood-2016-01-643569.
120. Remstein ED, Hanson CA, Kyle RA, Hodnefield JM, Kurtin PJ. Despite apparent morphologic and immunophenotypic heterogeneity, Waldenstrom's macroglobulinemia is consistently composed of cells along a morphologic continuum of small lymphocytes, plasmacytoid lymphocytes, and plasma cells. Semin Oncol. 2003;30:182–6. https://doi.org/10.1053/sonc.2003.50073.
121. Groves FD, Travis LB, Devesa SS, Ries LA, Fraumeni JF Jr. Waldenström's macroglobulinemia: incidence patterns in the United States, 1988-1994. Cancer. 1998;82(6):1078–81.
122. Kyle RA, Larson DR, McPhail ED, Therneau TM, Dispenzieri A, Kumar S, et al. Fifty-year incidence of Waldenström macroglobulinemia in Olmsted County, Minnesota, from 1961 through 2010: a population-based study with complete case capture and hematopathologic review. Mayo Clin Proc. 2018;93:739–46. https://doi.org/10.1016/j.mayocp.2018.02.011.
123. Thomas R, Braschi-Amirfarzan M, Laferriere SL, Jagannathan JP. Imaging of Waldenström macroglobulinemia: a comprehensive review for the radiologist in the era of personalized medicine. AJR Am J Roentgenol. 2019;213:W248–56. https://doi.org/10.2214/AJR.19.21493.
124. Fitsiori A, Fornecker LM, Simon L, Karentzos A, Galanaud D, Outteryck O, et al. Imaging spectrum of Bing-Neel syndrome: how can a radiologist recognise this rare neurological complication of Waldenström's macroglobulinemia? Eur Radiol. 2019;29:102–14. https://doi.org/10.1007/s00330-018-5543-7.
125. Hughes MS, Atkins EJ, Cestari DM, Stacy RC, Hochberg F. Isolated optic nerve, chiasm, and tract involvement in Bing-Neel Syndrome. J Neuroophthalmol. 2014;34:340–5. https://doi.org/10.1097/WNO.0000000000000138.
126. Minnema MC, Kimby E, D'Sa S, Fornecker LM, Poulain S, Snijders TJ, et al. Guideline for the diagnosis, treatment and response criteria for Bing-Neel syndrome. Haematologica. 2017;102:43–51. https://doi.org/10.3324/haematol.2016.147728.
127. Verdú J, Andrés R, Sánchez-Majano JL, Fernández JA. Bilateral ocular involvement as a presentation of Waldenström's macroglobulinemia. Med Oncol. 2011;28:1624–5. https://doi.org/10.1007/s12032-010-9648-3.
128. Krishnan K, Adams PT. Bilateral orbital tumors and lacrimal gland involvement in Waldenström's macroglobulinemia. Eur J Haematol. 1995;55:205–6. https://doi.org/10.1111/j.1600-0609.1995.tb00253.x.
129. Illarramendi OA, Flynt L, Wong F. 18F-FDG PET/CT in the evaluation of bing-neel syndrome. J Nucl Med Technol. 2019;47:343–4. https://doi.org/10.2967/jnmt.118.225565.
130. Eneh AA, Farmer J, Kratky V. Primary localized orbital amyloid: case report and literature review; 2004-2015. Can J Ophthalmol. 2016;51:e131–6. https://doi.org/10.1016/j.jcjo.2016.03.019.
131. Yerli H, Aydin E, Avci S, Haberal N, Oto S. Focal amyloidosis of the orbit presenting as a mass: MRI and CT features. Iran J Radiol. 2011;8:241–4. https://doi.org/10.5812/iranjradiol.4555.
132. Sipe JD, Benson MD, Buxbaum JN, Ikeda S, Merlini G, Saraiva MJ, et al. Nomenclature Committee of the International Society of Amyloidosis. Amyloid fibril protein nomenclature: 2012 recommendations from the Nomenclature Committee of the International Society of Amyloidosis. Amyloid. 2012;19:167–70. https://doi.org/10.3109/13506129.2012.734345.
133. Leibovitch I, Selva D, Goldberg RA, Sullivan TJ, Saeed P, Davis G, et al. Periocular and orbital amyloidosis: clinical characteristics, management, and outcome. Ophthalmology. 2006;113:1657–64. https://doi.org/10.1016/j.ophtha.2006.03.052.
134. Murdoch IE, Sullivan TJ, Moseley I, Hawkins PN, Pepys MB, Tan SY, et al. Primary localised amyloidosis of the orbit. Br J Ophthalmol. 1996;80:1083–6. https://doi.org/10.1136/bjo.80.12.1083.
135. Okamoto K, Ito J, Emura I, Kawasaki T, Furusawa T, Sakai K, et al. Focal orbital amyloidosis presenting as rectus muscle enlargement: CT and MR findings. AJNR Am J Neuroradiol. 1998;19:1799–801.
136. Haroche J, Arnaud L, Cohen-Aubart F, Hervier B, Charlotte F, Emile JF, et al. Erdheim-Chester disease. Curr Rheumatol Rep. 2014;16:412. https://doi.org/10.1007/s11926-014-0412-0.
137. Veyssier-Belot C, Cacoub P, Caparros-Lefebvre D, Wechsler J, Brun B, Remy M, et al. Erdheim-Chester disease. Clinical and radiologic characteristics of 59 cases. Medicine (Baltimore). 1996;75:157–69. https://doi.org/10.1097/00005792-199605000-00005.

138. Arnaud L, Hervier B, Néel A, Hamidou MA, Kahn JE, Wechsler B, et al. CNS involvement and treatment with interferon-α are independent prognostic factors in Erdheim-Chester disease: a multicenter survival analysis of 53 patients. Blood. 2011;117:2778–82. https://doi.org/10.1182/blood-2010-06-294108.
139. Drier A, Haroche J, Savatovsky J, Godenèche G, Dormont D, Chiras J, et al. Cerebral, facial, and orbital involvement in Erdheim-Chester disease: CT and MR imaging findings. Radiology. 2010;255:586–94. https://doi.org/10.1148/radiol.10090320.
140. Sedrak P, Ketonen L, Hou P, Guha-Thakurta N, Williams MD, Kurzrock R, et al. Erdheim-Chester disease of the central nervous system: new manifestations of a rare disease. AJNR Am J Neuroradiol. 2011;32:2126–31. https://doi.org/10.3174/ajnr.A2707.
141. Mamlouk MD, Aboian MS, Glastonbury CM. Case 245: Erdheim-Chester disease. Radiology. 2017;284:910–7. https://doi.org/10.1148/radiol.2017141151.
142. Nguyen VD, Singh AK, Altmeyer WB, Tantiwongkosi B. Demystifying orbital emergencies: a pictorial review. Radiographics. 2017;37:947–62. https://doi.org/10.1148/rg.2017160119.
143. Rahbar R, Robson CD, Petersen RA, DiCanzio J, Rosbe KW, McGill TJ, et al. Management of orbital subperiosteal abscess in children. Arch Otolaryngol Head Neck Surg. 2001;127:281–6. https://doi.org/10.1001/archotol.127.3.281.
144. Givner LB. Periorbital versus orbital cellulitis. Pediatr Infect Dis J. 2002;21:1157–8. https://doi.org/10.1097/00006454-200212000-00014.
145. Ansari SA, Mafee MF. Orbital cavernous hemangioma: role of imaging. Neuroimaging Clin N Am. 2005;15:137–58. https://doi.org/10.1016/j.nic.2005.02.009.
146. Bilaniuk LT. Vascular lesions of the orbit in children. Neuroimaging Clin N Am. 2005;15:107–20. https://doi.org/10.1016/j.nic.2005.03.001.
147. Katz SE, Rootman J, Vangveeravong S, Graeb D. Combined venous lymphatic malformations of the orbit (so-called lymphangiomas). Association with noncontiguous intracranial vascular anomalies. Ophthalmology. 1998;105:176–84. https://doi.org/10.1016/s0161-6420(98)92058-9.
148. Wright JE, Sullivan TJ, Garner A, Wulc AE, Moseley IF. Orbital venous anomalies. Ophthalmology. 1997;104:905–13. https://doi.org/10.1016/s0161-6420(97)30208-5.
149. Harris GJ, Sakol PJ, Bonavolontà G, De Conciliis C. An analysis of thirty cases of orbital lymphangioma. Pathophysiologic considerations and management recommendations. Ophthalmology. 1990;97:1583–92. https://doi.org/10.1016/s0161-6420(90)32370-9.
150. Smoker WR, Gentry LR, Yee NK, Reede DL, Nerad JA. Vascular lesions of the orbit: more than meets the eye. Radiographics. 2008;28:185–204. https://doi.org/10.1148/rg.281075040.
151. Graeb DA, Rootman J, Robertson WD, Lapointe JS, Nugent RA, Hay EJ. Orbital lymphangiomas: clinical, radiologic, and pathologic characteristics. Radiology. 1990;175:417–21. https://doi.org/10.1148/radiology.175.2.2326469.
152. Rubin PA, Remulla HD. Orbital venous anomalies demonstrated by spiral computed tomography. Ophthalmology. 1997;104:1463–70. https://doi.org/10.1016/s0161-6420(97)30115-8.
153. Winter J, Centeno RS, Bentson JR. Maneuver to aid diagnosis of orbital varix by computed tomography. AJNR Am J Neuroradiol. 1982;3:39–40.
154. Bigot JL, Iacona C, Lepreux A, Dhellemmes P, Motte J, Gomes H. Sinus pericranii: advantages of MR imaging. Pediatr Radiol. 2000;30:710–2. https://doi.org/10.1007/s002470000306.
155. Flors L, Leiva-Salinas C, Maged IM, Norton PT, Matsumoto AH, Angle JF, et al. MR imaging of soft-tissue vascular malformations: diagnosis, classification, and therapy follow-up. Radiographics. 2011;31:1321–40; discussion 1340–1. https://doi.org/10.1148/rg.315105213.
156. Ernemann U, Kramer U, Miller S, Bisdas S, Rebmann H, Breuninger H, et al. Current concepts in the classification, diagnosis and treatment of vascular anomalies. Eur J Radiol. 2010;75:2–11. https://doi.org/10.1016/j.ejrad.2010.04.009.
157. Donnelly LF, Adams DM, Bisset GS 3rd. Vascular malformations and hemangiomas: a practical approach in a multidisciplinary clinic. AJR Am J Roentgenol. 2000;174:597–608. https://doi.org/10.2214/ajr.174.3.1740597.
158. McCafferty IJ, Jones RG. Imaging and management of vascular malformations. Clin Radiol. 2011;66:1208–18. https://doi.org/10.1016/j.crad.2011.06.014.
159. Nosher JL, Murillo PG, Liszewski M, Gendel V, Gribbin CE. Vascular anomalies: a pictorial review of nomenclature, diagnosis and treatment. World J Radiol. 2014;6:677–92. https://doi.org/10.4329/wjr.v6.i9.677.
160. Abernethy LJ. Classification and imaging of vascular malformations in children. Eur Radiol. 2003;13(11):2483–97. https://doi.org/10.1007/s00330-002-1773-8.
161. Park HS, Gye HJ, Kim JM, Lee YJ. A patient with branch retinal vein occlusion accompanied by superior ophthalmic vein thrombosis due to severe superior ophthalmic vein enlargement in a patient with graves ophthalmopathy. J Craniofac Surg. 2014;25:e322–4. https://doi.org/10.1097/SCS.0000000000000586.
162. Gupta RK, Jamjoom AA, Devkota UP. Superior sagittal sinus thrombosis presenting as a continuous headache: a case report and review of the literature. Cases J. 2009;2:9361. https://doi.org/10.1186/1757-1626-2-9361.
163. Valera FC, dos Santos AC, Anselmo-Lima WT, Marquezini RM. Orbital complications of acute rhinosinusitis: a new classification. Braz J Otorhinolaryngol. 2007;73:684–8. https://doi.org/10.1016/s1808-8694(15)30130-0.